END
DATE
FILMED

DTIC

1.0

1.1

1.25

2.8   2.5

3.2   2.2

3.6

4.0   2.0

1.8

1.4   1.6

MICROCOPY RESOLUTION TEST CHART
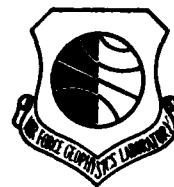NATIONAL BUREAU OF STANDARDS 1963 A

LEVEL II (12)

AFGL-TR-61-0102
ENVIRONMENTAL RESEARCH PAPERS, NO. 736

Radar Detection of Turbulence in Thunderstorms

ALAN R. BOHNE

DTIC
S ELECTE D
DEC 17 1981
E

31 March 1981

Approved for public release; distribution unlimited.

METEOROLOGY DIVISION   PROJECT 6670
AIR FORCE GEOPHYSICS LABORATORY
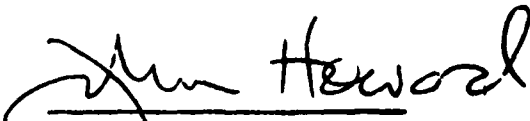HANSCOM AFB, MASSACHUSETTS 01731

AIR FORCE SYSTEMS COMMAND, USAF

81 12 17059

This report has been reviewed by the ESD Information Office (OI) and is releasable to the National Technical Information Service (NTIS).

This technical report has been reviewed and is approved for publication.

FOR THE COMMANDER

Chief Scientist

REPORT DOCUMENTATION PAGE	READ INSTRUCTIONS BEFORE COMPLETING FORM

1. REPORT NUMBER	2. GOVT ACCESSION NO.	3. RECIPIENT'S CATALOG NUMBER
AFGL-TR-81-0102	ADA108694	

4. TITLE (and Subtitle)	5. TYPE OF REPORT & PERIOD COVERED
RADAR DETECTION OF TURBULENCE IN THUNDERSTORMS	Scientific. Final.
	6. PERFORMING ORG. REPORT NUMBER
	ERP No. 736

7. AUTHOR(s)	8. CONTRACT OR GRANT NUMBER(s)
Alan R. Bohne	

9. PERFORMING ORGANIZATION NAME AND ADDRESS	10. PROGRAM ELEMENT, PROJECT, TASK AREA & WORK UNIT NUMBERS
Air Force Geophysics Laboratory (LYW) Hanscom Air Force Base Massachusetts 01731	62101F 66700604

11. CONTROLLING OFFICE NAME AND ADDRESS	12. REPORT DATE
Air Force Geophysics Laboratory (LYW) Hanscom Air Force Base Massachusetts 01731	31 March 1981
	13. NUMBER OF PAGES
	62

14. MONITORING AGENCY NAME & ADDRESS(if different from Controlling Office)	15. SECURITY CLASS. (of this report)
	Unclassified
	15a. DECLASSIFICATION DOWNGRADING SCHEDULE

16. DISTRIBUTION STATEMENT (of this Report)

Approved for public release; distribution unlimited.

17. DISTRIBUTION STATEMENT (of the abstract entered in Block 20, if different from Report)

18. SUPPLEMENTARY NOTES

19. KEY WORDS (Continue on reverse side if necessary and identify by block number)

Radar	Turbulence	Precipitation tracers
Doppler radar	Turbulence power spectrum	Precipitation response
Doppler spectrum mean	Turbulence outer scale	Aircraft gust velocity
Doppler spectrum variance	Eddy dissipation rate	

20. ABSTRACT (Continue on reverse side if necessary and identify by block number)

Theoretical investigations are undertaken to relate intensity of turbulent air motion to Doppler radar spectrum mean and variance in precipitation environments. Examples of theoretical radar derived turbulence power density spectra and total precipitation motion variance show that effects due to imperfect particle response are significant for turbulence scale lengths less than 250 m. Doppler spectrum variance and estimated eddy dissipation rate (ϵ) are found strongly dependent upon precipitation environment for ranges less than

DD FORM 1473
1 JAN 73

20. Abstract (Continued)

about 20 km, and for cases where the turbulence outer scale length (λ_0) is less than 0.5 km. They are also found to be essentially independent of λ_0 when the maximum pulse volume dimension is less than $1/2\ \lambda_0$, and independent of range but strongly dependent on λ_0 at ranges where the maximum pulse volume dimension is greater than λ_0. Estimation of ε by radar is shown to be unreliable until a method of remotely determining λ_0 is found. Nevertheless, classification of turbulence severity (index = $\varepsilon^{1/3}$) is possible with only a reasonable guess of λ_0. Analyses of aircraft gust velocity data indicate that thunderstorm turbulence is localized into discrete patches, and that such localization must be accounted for when aircraft gust velocity data undergo power spectrum analysis.

Contents

Illustrations

3

Radar Detection of Turbulence in Thunderstorms

1. INTRODUCTION

The detection of turbulence in thunderstorms by remote methods has been a
subject of investigation for many years. Early studies, relying on observations
from penetrating aircraft, attempted to correlate turbulence encounters with
radar storm features. The general conclusion was that the frequency of occur-
rence of moderate to severe turbulence increased markedly with increasing
storm radar echo intensity (dBZ), with 40 dBZ a rough threshold value for
development of such turbulence somewhere in the storm. Further observation
indicated that severe turbulence was widely distributed in storms whenever the
intensity indicated damaging hail (about 50 dBZ), with turbulence encounters
outside high intensity cores being as frequent as those within. [1] This was particu-
larly evident within thunderstorm lines where severe turbulence was frequently
encountered in low echo intensity regions between individual storms. The con-
clusion was that storm echo intensity was an indicator of the presence of turbu-
lence, but it did not reliably measure its strength nor locate its position.

In light of these results and with continued development in Doppler radar
techniques, emphasis was placed on finding kinematic signatures of hazardous

1. Lee, J. T. (1967) Atmospheric Turbulence and Radar Echoes in Oklahoma,
Technical Memorandum IERTM-NSSL 32, Norman, Oklahoma.

zones within thunderstorms. Armstrong and Donaldson[2] developed the Plan Shear Indicator (PSI), which was able to detect regions of strong shear of the radial wind. Lee and Kraus,[3] by comparing PSI and penetrating aircraft observations, found good correlation between regions of strong shear of the radial wind and severe turbulence events. Radar data of Frisch and Strauch[4] suggested that high turbulence intensity may not necessarily be correlated with zones of high shear of the radial wind, but when present, may be found in regions exhibiting large Doppler spectrum variance. Later Lee[5] also found good correlation between regions of severe turbulence and large spectrum variance. Thus, present attempts are being directed at using Doppler spectrum variance as a turbulence indicator.

The turbulent contribution to Doppler spectrum variance is a function of the turbulence intensity, range of the observation volume from the radar, and precipitation environment. Turbulence intensity may be related to the rate per unit mass at which turbulent kinetic energy is transferred from larger to smaller scales (eddy dissipation rate), and maximum eddy size (turbulence outer scale). The manner in which all these effects combine is not well known, thus the interpretation of this indicator is not yet completely understood. The aim of this research is to clarify the relationship between Doppler spectrum variance and these parameters, and to develop a more reliable radar turbulence detection technique.

This report focuses on results of theoretical investigations and data analyses performed during the period May, 1979 to the end of December 1980. Primary topics discussed are: 1) the response of a distribution of precipitation particles to various ranges of scales of turbulent motion; 2) the relationship between eddy dissipation rate and Doppler spectrum variance as a function of the turbulence scale regime and precipitation environment; 3) the distribution of local turbulence regimes within thunderstorms as delineated by aircraft data; and 4) the correlation of selected aircraft and radar data. Finally, since one of the ultimate goals of this work is to devise a methodology for turbulence detection by incoherent radar, a possible method by which non-Doppler radar may estimate wind shear

2. Armstrong, G., and Donaldson Jr., R. (1969) Plan shear indicator for real-time Doppler radar identification of hazardous storm winds, J. Appl. Meteor. 8:376-383.

3. Lee, J. T., and Kraus, M. (1975) Plan shear indicator and aircraft measurements of thunderstorm turbulence: experimental results, Preprints, 16th Radar Meteorology Conference, Amer. Meteor. Soc., Boston, pp. 337-340.

4. Frisch, A. S., and Strauch, R. G. (1976) Doppler radar measurements of eddy dissipation rates in a northeastern Colorado convective storm, J. Appl. Meteor. 15:1012-1017.

5. Lee, J. T. (1977) Application of Doppler Weather Radar to Turbulence Measurements Which Affect Aircraft, Final Report FAA-RD-77-145 to Systems Research and Development Service, FAA, Washington, D. C.

for the purpose of removing its contaminating effects from the Doppler spectrum variance will be briefly discussed. Results of these investigations point to the need for further data analysis for verification and selection of practical solutions.

2. THEORETICAL INVESTIGATIONS

The response of precipitation particles to turbulent air motions is of funda-
mental importance since the Doppler radar velocity is generally equated to the
radial component (the component along the radar viewing direction) of the envi-
ronmental wind. However, the Doppler power spectrum is formed from
measurements of the radial velocities of the precipitation particles within the
radar pulse volume, with the spectral power at each spectral velocity value
proportional to the sum of the sixth powers of the diameters of the precipitation
tracers moving with that radial velocity value. It is suspected that a sizable
portion of Doppler spectrum power may be supplied by tracers which, because
of their large inertia (for example, large raindrops), do not follow turbulent air
fluctuations faithfully. If this is so, then an incorrect estimate of the turbulent
air motion (for example, Doppler spectrum mean and variance) is obtained.
Thus, one is interested in determining the response of a distribution of particles
to various scales of motion. This may be obtained by appropriately summing the
individual responses of the particles comprising the distribution.

Consider a single particle. Its equation of motion may be written as

$$m_D \frac{d\vec{V}_D}{dT} = m_a \frac{d\vec{V}_a}{dT} + m_D \vec{g} \left(1 - \frac{\rho_a}{\rho_D}\right) - 3\pi D\mu(\vec{V}_D - \vec{V}_a) \frac{C_D N_{Re}}{24} \qquad (1)$$

where m_D, $\vec{V}_D$, ρ_D, and D are the mass, velocity, density, and diameter,
respectively, of the particle. Air density is ρ_a, m_a is the mass of displaced air,
and $\vec{V}_a$ is the undisturbed air velocity in the vicinity of the particle. Kinematic
viscosity is μ, gravitational acceleration is $\vec{g}$, and C_D and N_{Re} (= 2 Re) are the
drag coefficient and alternate Reynolds number of the particle. The coefficient
$C_D N_{Re}/24$ is a catchall term and is actually related to fluid acceleration and
past particle motion.[6] This equation simply relates the net force acting on the
particle to the pressure, buoyancy-corrected gravity, and drag terms.
Equation (1) may be written as

---

6. Pruppacher, H. R. and Klett, J. D. (1978) Microphysics of Clouds and
    Precipitation, D. Reidel Publishing Co., Boston.

9

$$\frac{d\vec{V}_D}{dT} = \frac{m_a}{m_D} \frac{d\vec{V}_a}{dT} + \vec{g} \left(1 - \frac{\rho_a}{\rho_D}\right) - (\vec{V}_D - \vec{V}_a)/\tau \qquad (2)$$

where

$$\tau = \frac{8 D \rho_D}{6 C_D |\vec{V}_D - \vec{V}_a| \rho_a} \, . \qquad (3)$$

Actual solution of Eq. (2) requires application of numerical methods, since C_D is dependent on $(\vec{V}_D - \vec{V}_a)$. To obtain a general analytic solution for the particle response it is necessary to make a simplifying assumption concerning the drag force. For this purpose it is assumed that, on the average, the particle is settling at its terminal fallspeed (V_T). The drag force in Eq. (2) may then be replaced by its average value.

Following Stackpole,[7] the following relation is then applicable:

$$\tau = \frac{V_T}{g} \, . \qquad (4)$$

Neglecting particle growth and the variation of air density with height, τ is a constant for each particle. Note that this assumption means that the drag coefficient is replaced by the value attained when the particle is settling at its normal terminal fallspeed in still air, and thus it is a slightly averaged particle response that may be estimated.

In applying Eq. (2) to a turbulent field, one generally considers turbulence as composed of a random collection of eddies having a range of scales (for example, wavelengths λ). Mathematically, one may view this collection as a series of harmonic functions of varying radian frequency (ω) or wavenumber ($|\vec{K}| = 2\pi/\lambda$), having random amplitude and combining to produce the observed turbulent structure. The response of a particle to a turbulent gust may therefore be considered the result of a superposition of the particle's responses to this collection of harmonic functions, or eddies.

The form of the particle response to a single such function may be seen by considering one dimension (horizontal) and introducing an air velocity

7. Stackpole, J. D. (1961) The effectiveness of raindrops as turbulence sensors, Proceedings 9th Weather Radar Conference, Amer. Meteor. Soc., Boston, pp. 212-217.

10

$$V_a = V_o e^{i\omega T} \tag{5}$$

into Eq. (2). The particle velocity is found to be

$$V_D = V_o \left((1 + \omega^2 \tau^2 \rho_o^2)^{1/2} / (1 + \omega^2 \tau^2)^{1/2} \right) e^{i(\omega T + ATAN \, \omega\tau(\rho_o - 1))} + A e^{-T/\tau} \tag{6}$$

where

$$\rho_o = \frac{\rho_a}{\rho_D} \quad .$$

Note that the solution for the vertical dimension has an additional vertical acceleration term g. The first term shows that the particle velocity is reduced in amplitude and phase shifted relative to the air velocity. The second term is a transient term and describes the time required to achieve this reduced amplitude, phase lagged, state of motion. The phase shift alone does not represent any energy loss for the particles. However, if the particles are entering a region of greater turbulent air energy (for example, a region dominated by larger eddies), then the transient period represents a time when the particles have less energy than they will exhibit once they have achieved their new state of oscillatory motion. On the other hand, if the particles are entering a region of decreased turbulent air energy dominated by smaller scale eddies, then the particles have excess energy during the transient period. Thus, on the average, the transient effects may not represent any net turbulence energy loss when compared to the hypothetical case where the particles have no transient period at all (where they attain their new state of motion instantaneously).

Furthermore, assuming the particles to be raindrops having a range of terminal fallspeeds of 1 m/sec to 9 m/sec, the transient term in Eq. (6) indicates that it would take 0.25 sec to 2 sec, or 0.25 m to 18 m distance fallen, to pass through the transient period. These lengths represent only the very lowest energy portion of the turbulence regimes of interest here (outer scale lengths of ≥ 500 m). Thus, the net transient energy loss should be very small indeed. Therefore, since the mathematical techniques involved here deal only with the average turbulent motion of a distribution of particles in relation to the average turbulent air energy, only the amplitude response term in Eq. (6) will be considered.

It is necessary to map this response function from dependence upon frequency to turbulence scale, since frequency is dependent upon the relative speed of the atmospheric structure and the sensing instrument (here the particles), and

11

therefore is an artificial turbulence parameter. In a manner similar to Taylor's hypothesis, one may form a relationship between turbulence wavenumber, radian frequency, and particle terminal fallspeed as

$$\omega = \vec{V}_T \cdot \vec{K} = V_T K_z \quad , \tag{7}$$

resulting in the response function taking the form

$$V_D/V_a = 1/(1 + K_z^2 V_T^4/g^2)^{1/2} \quad , \tag{8}$$

where $\rho_0 \approx 10^{-3}$ and $\omega \tau \rho_0 < 1$ have been assumed. This last condition is met for all rain and snow environments except for those combining large particle size and particle observed scales less than about 0.05 m. The energy content of the turbulent field at these scales is very small in relation to the larger scales of interest here and need not be considered further.

This relationship was first obtained by Stackpole[7] and states that as the particle size increases (V_T increases) the response to turbulent motions having any given apparent scale λ_a ($= K_z/2\pi$) decreases. Conversely, a particle of given size (V_T constant) exhibits decreasing response to decreasing scale. The term "apparent scale" has been used to signify that the particles are responding to the field which is the projection of the three dimensional turbulent field upon the z-axis and that there may not be a one to one correspondence of features in the three dimensional field to those observed in the one dimensional field.

To assess the effect imperfect particle response has upon the measurable radar parameters, it is necessary to modify the basic pertinent radar relations. In all that follows, the wind environment is considered fully turbulent, isotropic, and homogeneous. It is further assumed that the effects of Doppler spectrum broadening factors are additive and thus each contribution may be viewed separately. Here only the purely turbulent contribution will be investigated.

In general form the Doppler spectrum variance may be written as

$$VAR = \overline{V_p^2} - \overline{V}_p^2 \quad , \tag{9}$$

where V_p is particle radial velocity and the overbar indicates averaging over the Doppler power spectrum. This relation states that the spectrum variance equals the averaged square of particle radial velocity less the square of the averaged particle radial velocity. More specifically, this equation may be written as

$$\text{VAR} \quad \frac{C_1 \iint\limits_{\vec{R}} V_p^2(\vec{R}) q(V_p, \vec{R}) I(\vec{r}, \vec{R}) dV_p d\vec{R}}{C_1 \iint\limits_{\vec{R}} q(V_p, \vec{R}) I(\vec{r}, \vec{R}) dV_p d\vec{R}}$$

$$- \left[\frac{C_1 \iint\limits_{\vec{R}} V_p(\vec{R}) q(V_p, \vec{R}) I(\vec{r}, \vec{R}) dV_p d\vec{R}}{C_1 \iint\limits_{\vec{R}} q(V_p, \vec{R}) I(\vec{r}, \vec{R}) dV_p d\vec{R}} \right]^2 \tag{10}$$

showing more clearly the backscattered power averaging and pulse volume averaging over available particle radial velocities. Here C_1 is the radar constant, and $q(V_p, \vec{R})$ is the reflectivity density of the particles in the volume element $d\vec{R}$ (related to the sixth power of particle diameter, or melted diameter for snow) located $\vec{R}$ from the pulse volume center located at $\vec{r}$ (relative to the radar), and having radial velocities ranging from V_p to $V_p + dV_p$. The term $C_1 q(V_p, \vec{R}) I(\vec{r}, \vec{R}) d\vec{R} dV_p$ is the power backscattered by these particles to the radar, and $I(\vec{r}, \vec{R})$ is the two-way beam illumination pattern which is assumed normalized. The integral over $\vec{R}$ is the integral over the pulse volume, and the V_p integral is over the total unambiguous velocity range of the radar.

Generally, the precipitation backscattered power varies with position within the pulse volume; however, to incorporate the effect of imperfect response and make the above relation tractable, a simplifying assumption is required. It is assumed that during the time the radar samples a given region to form the sample data set (used to form the Doppler power spectrum), a characteristic distribution

$$N(D) = N_o e^{-\Lambda D} \tag{11}$$

of particles is swept past each point within the pulse volume. Here $N(D) \, dD$ is the number of particles per unit volume in the size range D to $D + dD$. In essence, this states that the reflectivity is constant throughout the pulse volume.

The air velocity at any given point within the pulse volume is the result of a superposition of various sized eddies to which each particle in the distribution has a definite response determined by its size. Thus, it is assumed that for a given eddy distribution, each point within the pulse volume has a well defined

13

relationship between particle Doppler speed and size. This allows the dependence upon particle velocity to be changed to dependence upon particle diameter

$$q(V_p, \vec{R})dV_p \rightarrow q(D)\,dD \tag{12}$$

and allows Eq. (10) to be rewritten as

$$VAR = \int_{\vec{R}} V_{pd}^2(\vec{R})I(\vec{r}, \vec{R})d\vec{R} - \left[\int_{\vec{R}} V_{pd}(\vec{R})I(\vec{r}, \vec{R})d\vec{R}\right]^2 , \tag{13}$$

where

$$V_{pd}^2(\vec{R}) = \frac{\displaystyle\int V_D^2(\vec{R})q(D)dD}{\displaystyle\int q(D)dD} \tag{14}$$

and

$$V_{pd}(\vec{R}) = \frac{\displaystyle\int V_D(\vec{R})q(D)dD}{\displaystyle\int q(D)dD} , \tag{15}$$

where $V_D(\vec{R})$ is the radial velocity of a given drop of diameter D located at the position $\vec{R}$ in the pulse volume.

This is essentially the classical definition of Doppler spectrum variance. However, the significant difference here is that $V_{pd}(\vec{R})$ is the reflectivity-weighted imperfect response of the particles, and thus incorporates the concept that during the sampling period, at a given point in space, the various size particles composing the particle distribution exhibit different velocities from each other and the single-valued air velocity at that point. With an ensemble (denoted by $\langle \; \rangle$) of observations, and noting that ensemble averaging mathematically is a summation and can be brought within the integral, Eq. (13) becomes

$$\langle VAR \rangle = \langle [V_{pd}^2] \rangle - \langle [V_{pd}]^2 \rangle = \langle V_{pd}^2 \rangle - VAR([V_{pd}]) , \tag{16}$$

14

where now the bracket indicates averaging over the pulse volume (note that $\langle [V_{pd}] \rangle$, the average Doppler spectrum mean velocity in the turbulent field, is zero). This states that the average Doppler spectrum variance equals the average one-dimensional reflectivity-weighted particle turbulent motion variance minus the average variance of the Doppler mean velocity. This is a modification of the relation of Rogers and Tripp.[8] It is important to note here that this radar mean particle turbulent variance is not the air turbulent variance, but the reflectivity-weighted response of the particle distribution to the air turbulent motions. Similarly, the Doppler mean velocity term also includes the imperfect response function.

To incorporate the response functions it is useful to transform Eq. (16) into wavevector space. Srivastava and Atlas[9] have shown that the average variance of the Doppler spectrum (Eq. [16], for the case of a uniform distribution of perfect tracers) is given by

$$\langle VAR \rangle = \int_{\vec{K}} \phi_{11}(\vec{K})(1 - \phi_{I}(\vec{K})) \, d\vec{K} \quad , \tag{17}$$

where $\vec{K}$ is the three-dimensional turbulent wavevector, $\phi_{I}(\vec{K}) = (2\pi)^{6} F_{I}(\vec{K}) F_{I}^{*}(\vec{K})$, where $F_{I}(\vec{K})$ is the Fourier transform of $I(\vec{r}, \vec{R})$, and $\phi_{11}(\vec{K})$ is the turbulent power density function of the radial (1) air velocity component. Equation (17), however, does not include the particle response functions. Referring back to Eqs. (13) through (15), the new modified form of this relation becomes

$$\langle VAR \rangle = \int_{\vec{K}} \phi_{11}(\vec{K})(R_{2}(K_{z}) - R_{1}(K_{z})\phi_{I}(\vec{K})) \, d\vec{K} \tag{18}$$

$$R_{2}(K_{z}) = \int \frac{e^{-\Lambda D} D^{6} \, dD}{(1 + K_{z}^{2}(aD^{b})^{4}/g^{2})} \bigg/ \int e^{-\Lambda D} D^{6} \, dD \tag{19}$$

8. Rogers, R. R., and Tripp, B. R. (1964) Some radar measurements of turbulence in snow, J. Appl. Meteor. 3:603-610.

9. Srivastava, R. C., and Atlas, D. (1974) Effect of finite radar pulse volume on turbulence measurements, J. Appl. Meteor. 13:472-480.

and

$$R_1(K_z) = \left[\int \frac{e^{-\Lambda D} D^6 \, dD}{(1 + K_z^2(aD^b)^4/g^2)^{1/2}} \bigg/ \int e^{-\Lambda D} D^6 \, dD \right]^2 \quad . \tag{20}$$

The particle fallspeed has been replaced by

$$V_T = a D^b \quad , \tag{21}$$

where D is particle diameter (or melted particle diameter) and a, b are constants. The reflectivity weighted (D^6 weighting) imperfect response function is now explicitly shown. The terms $R_2(K_z)$, $R_1(K_z)$ are the particle turbulent motion variance and turbulent velocity weighting factors, respectively.

In Eq. (18), $\phi_{11}(\vec{K})$ essentially describes the actual one-dimensional turbulent air motion intensity as a function of turbulent scale. Multiplication of this by $R_2(K_z)$ results in the description of maximum radar measurable one-dimensional particle motion variance as a function of turbulent scale. Multiplying $\phi_{11}(\vec{K})$ by $R_1(K_z)\phi_I(\vec{K})$ describes how much of this radar measurable precipitation motion is mapped into fluctuation of the mean Doppler velocity. In both cases, the action of the response function is to pass along, relatively unscathed, the large scale turbulent motions to the precipitation, while severely limiting the small scale turbulent motions. The average Doppler spectrum variance is simply the difference between the maximum one-dimensional radar measurable precipitation motion variance and the average variance of the fluctuation of the Doppler mean velocity about the ensemble average of zero. This is the desired result.

There are a few points to note in Eq. (18). First, the results are dependent only on the slope (Λ) of the particle distribution function and not on the actual particle concentration number N_0. Secondly, if the pulse volume is decreased in size to a point (in which case the beam filter function $\phi_I[\vec{r}, \vec{R}]$ behaves as a delta function, for which $\phi_I[\vec{K}]$ becomes unity over all $\vec{K}$,), there exists a minimum variance which must always be observed. Its value is given by

$$\langle VAR \rangle_{min} = \int_{\vec{K}} \phi_{11}(\vec{K})(R_2(K_z) - R_1(K_z)) \, d\vec{K} \quad . \tag{21}$$

Numerical calculations show that this term is small and reflects the fact that the two weighting functions are nearly identical in net effect. The existence of

16

this minimum variance is expected, since the point in space (now representing the pulse volume) is observed for a finite amount of time, during which a distribution of particles having differing radial velocities (because of varying response characteristics) sweeps by and contributes to the Doppler power spectrum.

The variation of these response functions with wavenumber component K_z is shown in Figures 1a and 1b for various particle distribution slopes. The particles are assumed to be raindrops with the constants in Eq. (21) set at

$$a = 1690 \ cm^{0.4} \quad and \quad b = 0.6 \quad .$$

These figures show that the reflectivity-weighted precipitation response is good for turbulent motions having an apparent scale λ_a (measured along the z-direction) larger than about 250 m, with virtually no response to scales of motion smaller than about 10 m. As expected, better response is obtained in light rain ($\Lambda = 60 \ cm^{-1}$) than in heavy rain ($\Lambda = 20 \ cm^{-1}$) environments. It should also be remembered that the response, although excellent, is not perfect for scales greater than 1 km.

To foster a better appreciation for the effects of these response functions, it is useful to compare the maximum three-dimensional precipitation motion variance measurable by radar ($\langle VAR \rangle_{rm}$) and that actually contained by the particles ($\langle VAR \rangle_m$). The radar measurable quantity demonstrates $R_2(K_z)$ and could be the sum of the mean Doppler spectrum variance and average variance of the mean Doppler velocity from three radars observing the same location from orthogonal directions. The mechanical precipitation variance demonstrates Eq. (8). The maximum three-dimensional mechanical turbulent motion variance is given by

$$\langle VAR \rangle_m = \langle u^2 + v^2 + w^2 \rangle_m = \int E(K)W(K) \ dK \quad , \tag{23}$$

where the air energy density $E(K)$ is assumed given by the Kolmogorov relation

$$E(K) = C \ \varepsilon^{2/3} K^{-5/3} \tag{24}$$

in which C is a known constant, ε is the eddy dissipation rate, and $K = |\vec{K}|$. The particle distribution response is

$$W(K) = 2\int \left\{ \left[gN(D)atan(KV_T^2/g) \right] / KV_T^2 \right\} dD \bigg/ \int N(D) \ dD \quad , \tag{25}$$

this minimum variance is expected, since the point in space (now representing the pulse volume) is observed for a finite amount of time, during which a distribution of particles having differing radial velocities (because of varying response characteristics) sweeps by and contributes to the Doppler power spectrum.

The variation of these response functions with wavenumber component K_z is shown in Figures 1a and 1b for various particle distribution slopes. The particles are assumed to be raindrops with the constants in Eq. (21) set at

$$a = 1690 \text{ cm}^{0.4} \quad \text{and} \quad b = 0.6 \quad .$$

These figures show that the reflectivity-weighted precipitation response is good for turbulent motions having an apparent scale λ_a (measured along the z-direction) larger than about 250 m, with virtually no response to scales of motion smaller than about 10 m. As expected, better response is obtained in light rain ($\Lambda = 60 \text{ cm}^{-1}$) than in heavy rain ($\Lambda = 20 \text{ cm}^{-1}$) environments. It should also be remembered that the response, although excellent, is not perfect for scales greater than 1 km.

To foster a better appreciation for the effects of these response functions, it is useful to compare the maximum three-dimensional precipitation motion variance measurable by radar ($\langle VAR \rangle_{rm}$) and that actually contained by the particles ($\langle VAR \rangle_m$). The radar measurable quantity demonstrates $R_2(K_z)$ and could be the sum of the mean Doppler spectrum variance and average variance of the mean Doppler velocity from three radars observing the same location from orthogonal directions. The mechanical precipitation variance demonstrates Eq. (8). The maximum three-dimensional mechanical turbulent motion variance is given by

$$\langle VAR \rangle_m = \langle u^2 + v^2 + w^2 \rangle_m = \int E(K)W(K) \, dK \quad , \tag{23}$$

where the air energy density $E(K)$ is assumed given by the Kolmogorov relation

$$E(K) = C \, \varepsilon^{2/3} K^{-5/3} \tag{24}$$

in which C is a known constant, ε is the eddy dissipation rate, and $K = |\vec{K}|$. The particle distribution response is

$$W(K) = 2\int \left\{ \left[gN(D)\text{atan}(KV_T^2/g) \right] / KV_T^2 \right\} dD \bigg/ \int N(D) \, dD \quad , \tag{25}$$
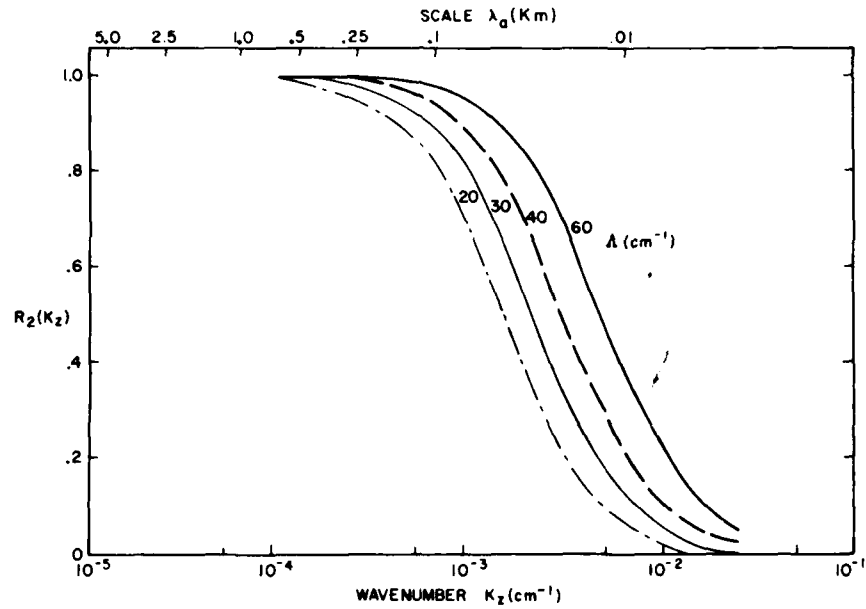
Figure 1a. Precipitation Response Function $R_2(K_z)$ for Precipitation Environments of Λ = 20 to 60 cm^{-1}. Apparent space scale at top
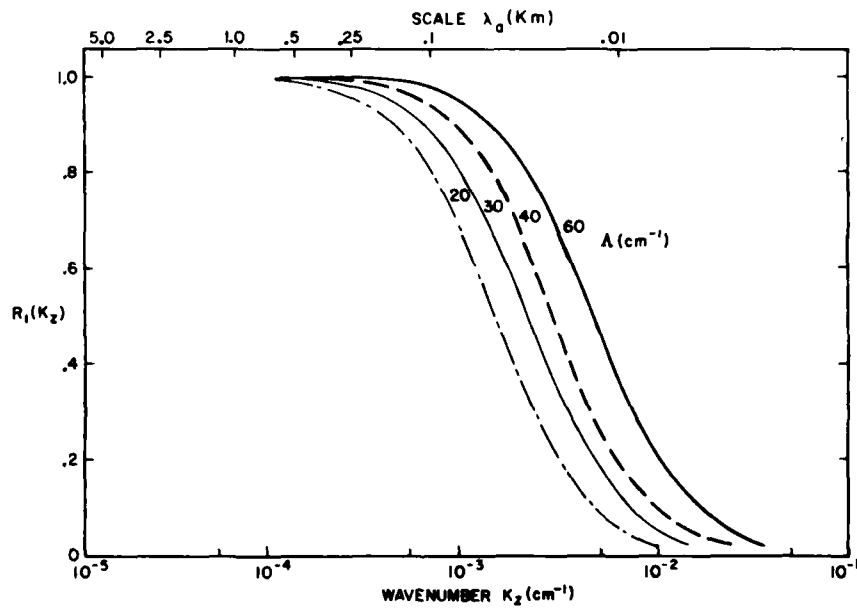

Figure 1b. Precipitation Response Function $R_1(K_z)$ for Precipitation Environments of Λ = 20 to 60 cm^{-1}. Apparent space scale at top

18

where the particle number density and fallspeed are given by Eqs. (11) and (21), respectively. Figure 2 shows this variance $\langle VAR \rangle_m$, normalized to the air motion variance $\langle VAR \rangle_a$ where

$$\langle VAR \rangle_a = 2 \int E(K) \, dK \quad . \tag{26}$$

The constant parameters in Eqs. (23) through (26) are $a = 1690 \text{ cm}^{0.4} \text{ sec}^{-1}$, $b = 0.6$, $D_{min} = 0.005 \text{ cm}$, $D_{max} = 0.5 \text{ cm}$, and $K_{max} = 2\pi \text{cm}^{-1}$ (corresponding to a minimum turbulence scale of 1 cm). Parameters K_{min} ($= 2\pi/\lambda_0$) corresponding to a turbulence outer scale λ_0 and the particle distribution slope Λ are the independent variables.

This figure shows that the mean turbulent variance of the particles is typically 95 percent (or greater) of the air value, for all precipitation environments (for example, heavy rain $\Lambda = 10 \text{ cm}^{-1}$ to light rain $\Lambda = 60 \text{ cm}^{-1}$) and outer scales ($\lambda_0$) greater than 500 m.

This figure demonstrates that even though individual particles (for example, large drops) may not respond well to small scales of motion, the actual mean turbulent velocity variance of the particle distribution is generally a good measure of the atmospheric value. Unfortunately, the radar does not weight the particles identically, as this calculation assumes, but rather weights the particles according to the sixth power of drop diameter.

The maximum three-dimensional radar measurable turbulent variance is given by

$$\langle VAR \rangle_{rm} = \langle u^2 + v^2 + w^2 \rangle_{rm} = \int E(K) W_1(K) \, dK \quad , \tag{27}$$

where

$$W_1(K) = 2 \int \left\{ \left[gN(D)D^6 \operatorname{atan}(KV_T^2/g) \right] / KV_T^2 \right\} dD \Big/ \int N(D) D^6 dD \quad . \tag{28}$$

This quantity, normalized to the actual turbulent air variance, is shown in Figure 3. It is observed that if the outer scale (λ_0) extends to a kilometer or more, then the radar can measure 90 to 97 percent of the air motion variance in all precipitation environments. For shorter outer scales, however, particularly in heavy rain situations, the radar estimate may be in significant error. As an example, for $\Lambda = 10 \text{ cm}^{-1}$ and an outer scale of 250 m, the total radar measurable variance

19

OUTER SCALE λ_o(Km)

.1   .167   .25   .4   1.0   2.0   4.0

$\Lambda = 60\ cm^{-1}$

$\Lambda = 10\ cm^{-1}$

$K_{max} = 2\pi\ cm^{-1}$

1.0
.9
.8
.7
.6

$\dfrac{VAR_m}{VAR_a}$

10^{-5} 10^{-4} 10^{-3}

MINIMUM WAVENUMBER K_{min} (cm^{-1})
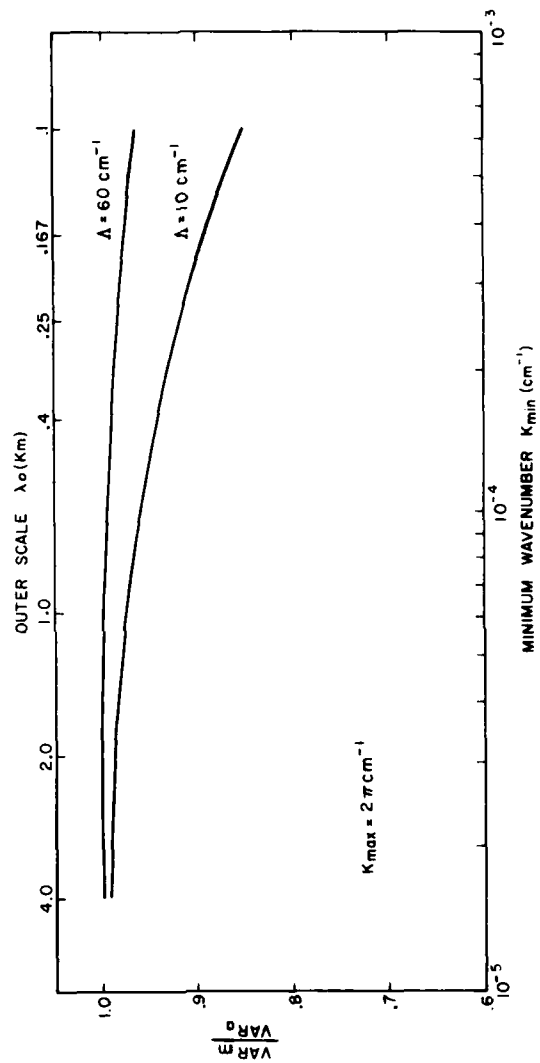
Figure 2. Ratio of Total (3-D) Precipitation Motion Variance $\langle VAR \rangle_m$ to Air Motion Variance $\langle VAR \rangle_a$ For Precipitation Environments Λ 10 to 60 cm^{-1} Versus Minimum Total Wavevector Magnitude. Turbulent outer scale at top
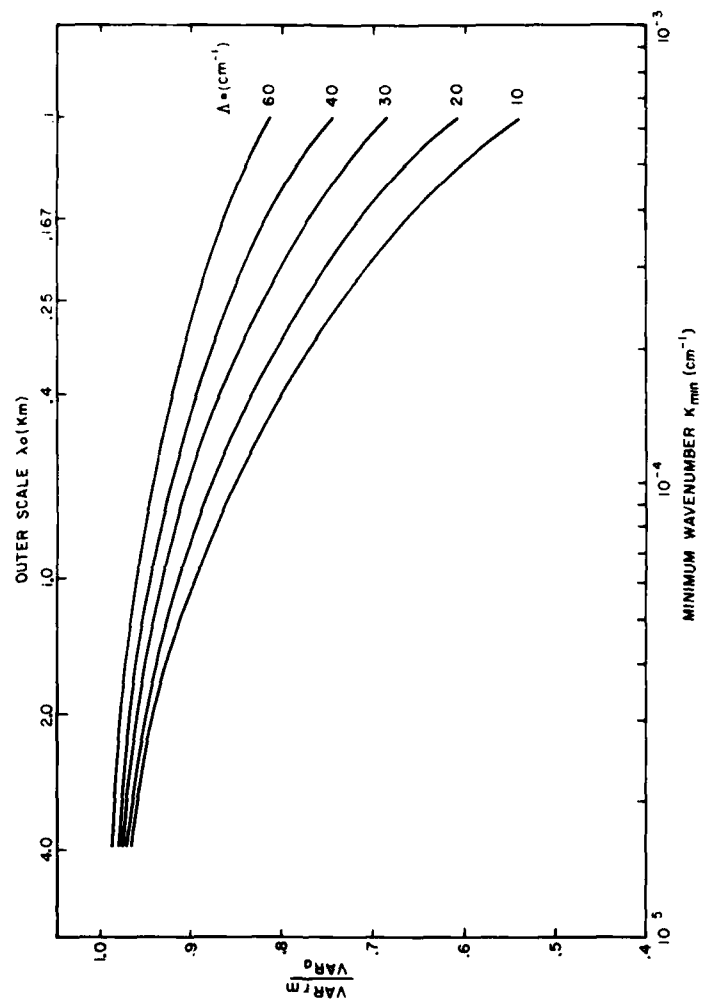
20

Figure 3. Ratio of Total (3-D) Radar Measurable Turbulent Motion Variance $\langle VAR \rangle_{rm}$ to Air Motion Variance $\langle VAR \rangle_a$ Versus Minimum Total Wavevector Magnitude in Precipitation Environments $\Lambda = 10$ to $60 \ cm^{-1}$. Turbulent outer scale at top

21

is only about 72 percent of the air value. The striking difference between Figures 2 and 3 results from the strong power contribution to the Doppler spectrum from large particles which exhibit poor response characteristics, and demonstrates that the usual assumption of precipitation being perfect tracers of the air motion can lead to radar turbulence energy estimates having significant error. The results demonstrate that imperfect particle response and the finite outer scale of turbulence must be taken into account if reasonable estimates of turbulence parameters are to be obtained by radar methods.

It was stated that the available radar measurable precipitation motion variance is partitioned between the average Doppler spectrum variance and the average variance of the fluctuating Doppler velocity. This effect may best be illustrated by graphical presentation of the two terms forming the right side of Eq. (18). For mathematical ease, the viewing direction is chosen as vertical. The radial direction (1) now becomes the z direction. The resulting average Doppler spectrum variance relation (Eq. [18]) may be written as

$$\langle \text{VAR} \rangle = \int (\phi_{zz}(K_z)R_2(K_z) - \phi_{zzf}(K_z)R_1(K_z)) \, dK_z \quad , \tag{29}$$

where

$$\phi_{zz}(K_z) = \iint \phi_{zz}(\vec{K}) dK_x dK_y \tag{30}$$

$$\phi_{zzf}(K_z) = \iint \phi_{zz}(\vec{K})\phi_I(\vec{K}) dK_x dK_y \tag{31}$$

and

$$\phi_{zz}(\vec{K}) = \left(1 - \frac{K_z^2}{K^2}\right) \frac{E(K)}{4\pi K^2} \quad . \tag{32}$$

Here $\phi_{zz}(K_z)$ is the true turbulent air one-dimensional longitudinal power density spectrum function along the z-direction. Similarly, $\phi_{zzf}(K_z)$ represents the spectrum that would result from power spectrum analysis of Doppler radial velocities obtained from a set of successive range bins (close enough so that the pulse volume dimensions may be considered constant) along the radial at some range r from the radar in an environment of a uniform distribution of perfect tracers.

22

Figures 4a and 4b show the two components to ϕ this one-dimensional representation for the two cases of outer scale λ_o $\neq$ 1 km. The radar is assumed to have a full half-power beamwidth of 1 degree and the pulse volume depth is 200 m. The outer curve (labeled pt) is the true turbulent air spectrum $\phi_{zz}(K_z)$ [Eq. (30)] and theoretically represents the spectrum that would be obtained from power spectrum analysis of the Doppler velocities from successive point (pt) sized pulse volumes along the z-direction in an environment of perfect tracers (air). The lower curves (labeled 5, 20, 40, 60, 120) are the corresponding radar pulse volume filtered turbulent air (perfect tracer) spectra $\phi_{zzf}(K_z)$ [Eq. (31)] for the five ranges mentioned. The curves labeled pt Λ $=$ 10 cm^{-1} or pt Λ $=$ 60 cm^{-1} represent the modifications to the true turbulent air spectra for rain environments having Λ $=$ 10 cm^{-1} and Λ $=$ 60 cm^{-1} and represent the $\phi_{zz}(K_z)R_2(K_z)$ term in Eq. (29). The curve labeled 20 km Λ $=$ 10 cm^{-1} is the turbulence power spectrum that would result when the pulse volume dimensions are those of a real pulse volume located 20 km from the radar, and is representative of the true radar measurement. The imperfect tracer curves for ranges greater than 20 km are nearly identical to the respective perfect tracer (air) curves and are not drawn. This last effect simply reflects the better response of the precipitation particles to the dominant contributing scales, which are increasing with increasing pulse volume size. These curves show the reduction of turbulence energy at small apparent spectral scales (large K_1) due to imperfect precipitation response. This indicates that as researchers reduce the observation range to reduce the effects of pulse volume filtering, they must pay greater attention to the effect imperfect precipitation response will have on their derived turbulence power spectra.

The curves also show that the "knee" of the curves (Figure 4b) are a good indication of the turbulence outer scale length for this isotropic field [Eq. (32)]. We will next return to the task of extracting useful turbulence information from the Doppler spectrum variance.

The Doppler spectrum variance [Eq. (29)] is the areal difference between the appropriate point and range spectral curves (Figure 4b but plotted on linear scales). For example, in a perfect tracer (air) environment having a turbulence outer scale λ_o = 1 km, the Doppler spectrum variance for the case where the radar is observing a region 20 km away is the areal difference between the air point curve and air 20 km curve in Figure 4b. Similarly, in a rain environment having Λ = 10 cm^{-1}, the Doppler spectrum variance is the areal difference between the pt Λ = 10 cm^{-1} curve and the 20 km Λ = 10 cm^{-1} curve. It should be noted that for ranges greater than about 20 km, the pulse volume filtered spectra for air (ϕ_{zzf}) may be substituted for the precipitation environment curve ($\phi_{zzf}R_1$) with negligible error.

To determine whether the interpretations from the vertical observations can be extended to the horizontal direction, calculations were performed to investigate the
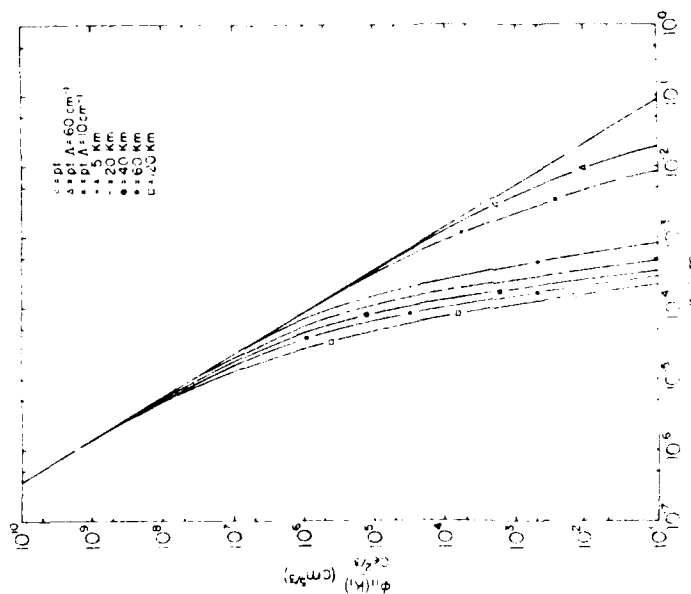
23

Figure 4b. Longitudinal Turbulence Power Spectrum. Outer Scale Length is λ_0 = 1 km. Radial (1) direction chosen as vertical (v). Curve labeled pt represents true air spectrum $o_{zz}(K_z)$. Curves labeled at Λ = 10, 60 cm^{-1} are equivalent spectra $o_{zz}(K_z)$ $R_2(k)$, for precipitation environments of Λ = 10, 60 cm^{-1}. Curves labeled 5, 20, 40, 60, 120 km are radar beam filtered spectra $(o_{zz}(K_z))$ for air for ranges mentioned. Full half-power beamwidth is 1° and pulse volume depth is 200 m.

Figure 4a. Longitudinal Turbulence Power Spectrum. Outer Scale Length is λ_0 = 1020 km. Radial (1) direction chosen as vertical (v). Curve labeled pt represents true air spectrum $o_{zz}(K_z)$. Curves labeled pt Λ = 10, 60 cm^{-1} are equivalent spectra $o_{zz}(K_z)R_2(k)_z$ for precipitation environments of Λ = 10, 60 cm^{-1}. Curves labeled 5, 20, 40, 60, 120 km are radar beam filtered spectra $(o_{zz}(K_z))$ for air for ranges mentioned. Full half-power beamwidth is 1° and pulse volume depth is 200 m.
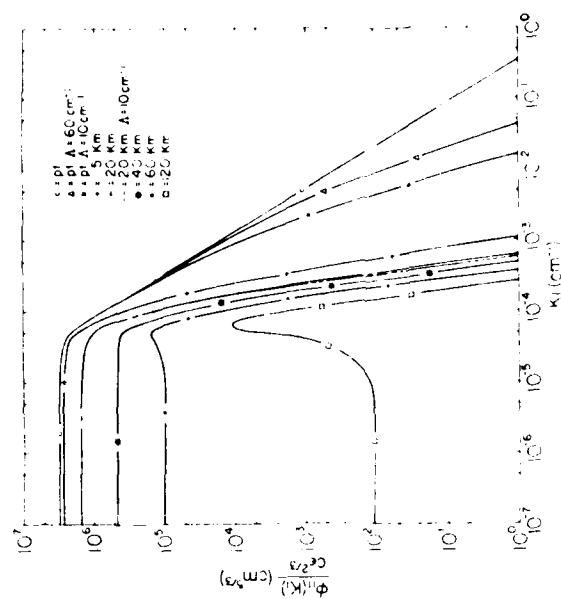
24

partitioning of the total radar measurable motion variance $(\langle u^2 \rangle + \langle v^2 \rangle + \langle w^2 \rangle)_{rm}$ among the three orthogonal components. The analysis shows that in light rain situations, this quantity was partitioned equally between the x y z components. In heavy rain environments, however, the horizontal variance components were noticeably smaller than the vertical component for turbulence outer scale lengths less than about 0.25 km (for example, $\langle u^2 \rangle / \langle w^2 \rangle$ = 0.95, 0.91, 0.88 for λ_o = 0.5, 0.25, 0.167 km respectively). This is a real effect and results from the horizontal and vertical power density spectra having a different K_z dependence, while the response function of the particle distribution is dependent only upon K_z. A more exact form of the response function allowing for some slight dependence upon K_x, K_y would presumably retain greater equality among the three component motion variances to shorter outer scale values.

To determine the relevance of these numbers, consider the longitudinal power density spectra that would be obtained by looking along the x and z directions in a turbulent environment with λ_o 1 km. For the case of perfect tracers (air), the spectra $o_{xx}(K_x)$ and $o_{zz}(K_z)$ are identical to the air point curve in Figure 4b. Note that the area below each curve would be $\langle u^2 \rangle = \langle w^2 \rangle$. Now, introduction of precipitation will produce the modified point curves $o_{xx}(K_x)R_2(K_z)$ and $\phi_{zz}(K_z)R_2(K_z)$. If Λ = 10 cm^{-1}, the vertical direction curve is identical to the pt Λ = 10 cm^{-1} curve in Figure 4b. However, because of the different K_z dependence of the horizontal turbulence spectrum, the pt Λ = 10 cm^{-1} curve for the horizontal direction will be slightly different. Similarly, for finite observation ranges, the u and w (Figure 4b) curves will continue to exhibit slight differences. However, the near equality $(\langle u^2 \rangle \doteq \langle w^2 \rangle)$ for cases where λ_o > 0.25 km suggests that the differences in the u and w precipitation environment longitudinal power spectral curves will be at very low apparent scale (large K_x, K_z) values. For finite ranges, pulse volume filtering dominates over precipitation response effects, thus the difference in Doppler spectrum variances results primarily from the difference in the modification of the point curves which is known to be small. These results indicate that solution of Eq. (25) yields the Doppler spectrum variance that would be measured along any viewing direction in any precipitation environment exhibiting turbulence outer scale values of 0.25 km or greater.

Numerical evaluation of Eq. (29) was performed to estimate the Doppler spectrum variance that would be obtained in a variety of precipitation and turbulent environments. Figures 5a and 5b show the variance (normalized to $C \epsilon^{2/3}$) versus the range, and the ratio of pulse volume width to depth. The solid, long dash, and short dash curves represent the air (perfect tracer) and imperfect tracer (Λ = 60, 10 cm^{-1}) environments respectively. The curve marked $\lambda_o = \infty$ is essentially

Figure 5a. Doppler Spectrum Variance ⟨VAR⟩ Normalized
to $C\varepsilon^{2/3}$ Versus Radar Range. Turbulence Outer Scale
Lengths are λ_o = 1, 4, ∞ km. Full half-power beamwidth
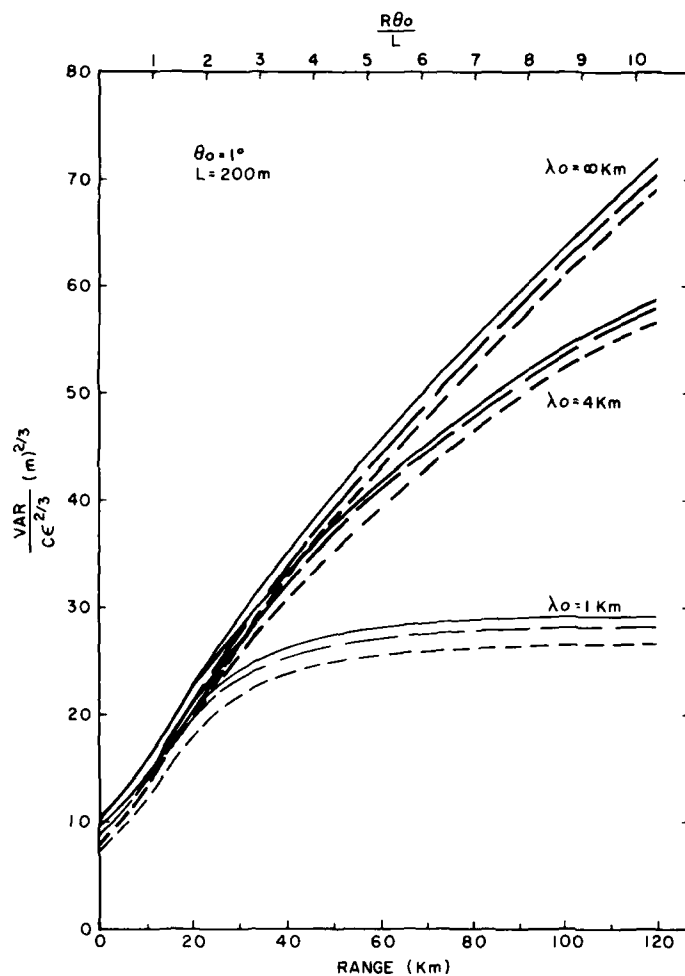is 1° and pulse volume depth is 200 m. Ratio of pulse vol-
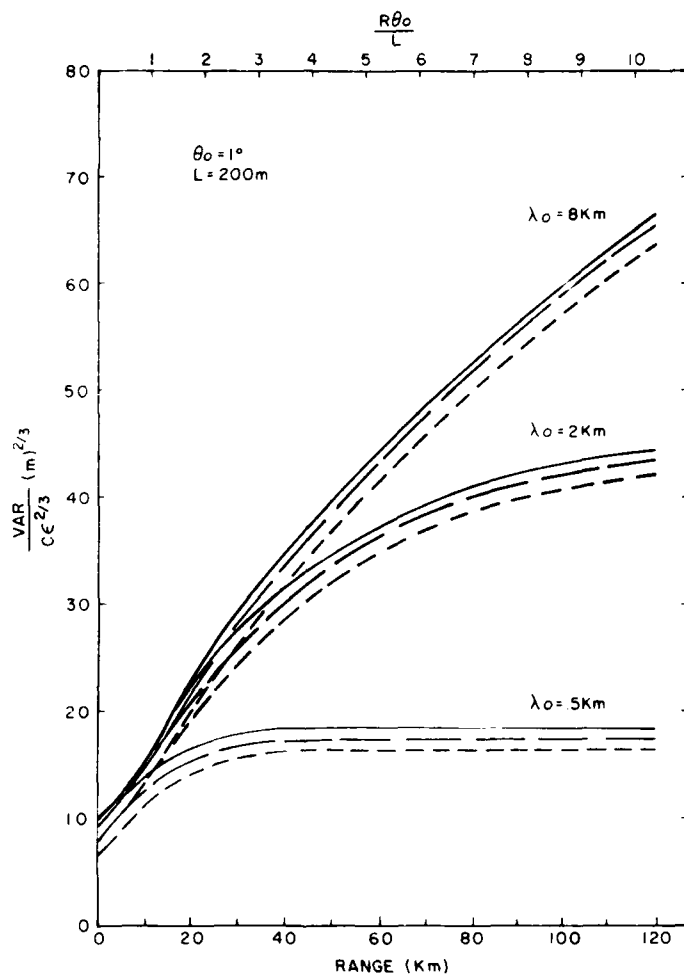ume width to depth ratio at top

26

Figure 5b. Doppler Spectrum Variance (VAR) Normalized
to $C\epsilon^{2/3}$ Versus Radar Range, Turbulence Outer Scale
Lengths are λ_o = 0.5, 2, 8 km.   Full half-power beamwidth
is 1° and pulse volume depth is 200 m.   Ratio of pulse vol-
ume width to depth ratio at top

Figure 4a and is well represented by a corrected form of the analytical approximation of Frisch and Clifford.[10] It is noted that the spectrum variance is essentially independent of outer scale length for ranges less than about 20 km. This simply reflects that at short ranges the various turbulent fields are nearly indistinguishable to the relatively small (compared to outer scale size) pulse volume, and the variance contribution can be reasonably estimated from the corrected form of the approximation of Frisch and Clifford.[10] Significant deviation from this relation occurs when the maximum pulse volume dimension approaches the outer scale value. When the maximum pulse volume dimension becomes larger than the turbulence outer scale, nearly all turbulent motion is mapped into Doppler spectrum variance. As radar range increases beyond this point, the Doppler variance becomes constant, independent of range.

The variation due to precipitation environment is significantly smaller, with increasing dependence on rain environment occurring with decreasing outer scale size and decreasing range. These features can more easily be seen by inverting the figures to form the estimate for eddy dissipation rate, the fundamental turbulence parameter.

Figures 6a and 6b show ϵ normalized to $((VAR\ C)^{3/2}$ as a function of range, the pulse volume width depth ratio, outer scale λ_o, and particle distribution slope Λ. Observe that the precipitation effects become less important as the turbulence outer scale length increases. This reflects the more favorable response of the particles to increasing turbulence scale lengths, which also contain increasingly greater portions of the total turbulent air energy. Furthermore, precipitation effects become less pronounced with increasing range. For example, in heavy rainfall ($\Lambda \approx 10$ cm^{-1}) in a turbulent environment having a turbulence outer scale of 0.5 km the assumption of no precipitation results in an underestimate of ϵ of 42 and 20 percent at ranges of 5 and 40 km. For a turbulence outer scale of 2 km, the corresponding underestimates are 28 and 1 percent. In light rain situations, the underestimates are about half these values. Thus, in situations where the range is short (perhaps less than 20 km), or where the turbulence outer scale is expected to be small (for example, breaking Kelvin-Helmholtz waves), it is important that the precipitation environment be taken into account.

What these figures further imply, however, is that without some reasonable knowledge of the turbulence outer scale length, estimation of eddy dissipation rate and correction for precipitation effects may be a fruitless exercise. In stratiform type snow or rain situations, both the Doppler spectrum mean and variance would generally be used to determine the turbulence outer scale and eddy dissipation rate.

10. Frisch, A.S., and Clifford, S.F. (1974) A study of convection capped by a stable layer using Doppler radar and acoustic echo sounders, J. Atmos. Sci. 31:1622-1628.

Figure 6a. Eddy Dissipation Rate Normalized to
$(\langle VAR \rangle /C)^{3/2}$ Versus Radar Range, Turbulence
Outer Scale Length are $\lambda_o = 1, \infty$ km. Radar
full half-power beamwidth is 1° and pulse volume
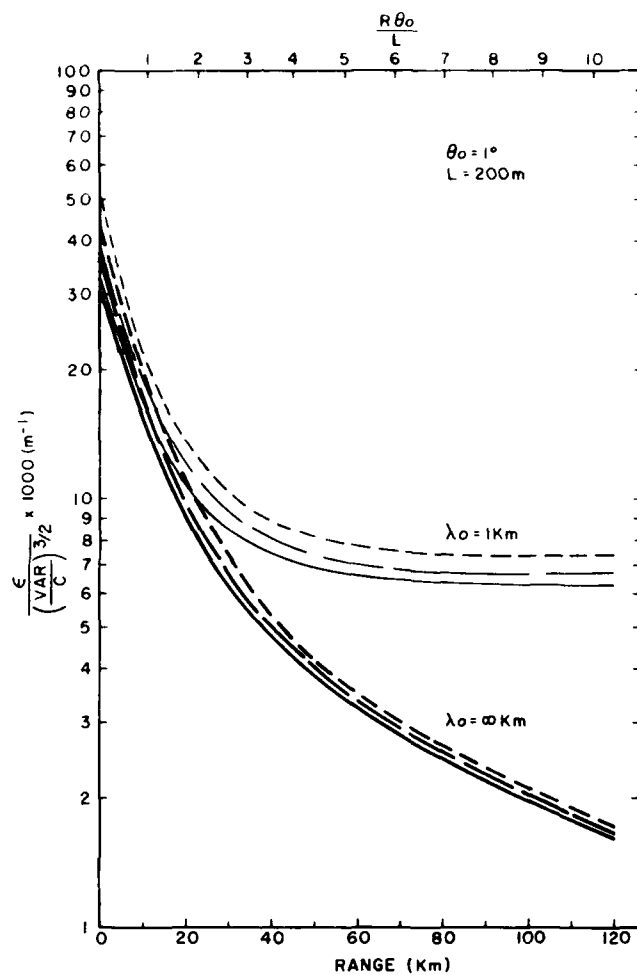depth is 200m. Ratio of pulse volume to depth at
top

Figure 6b. Eddy Dissipation Rate Normalized to $(\langle VAR \rangle / C)^{3/2}$ Versus Radar Range, Turbulence Outer Scale Length are $\lambda_0 = 0.5$, 4 km. Radar full half-power beamwidth is 1° and pulse volume depth is 200 m. Ratio of pulse volume to depth at top
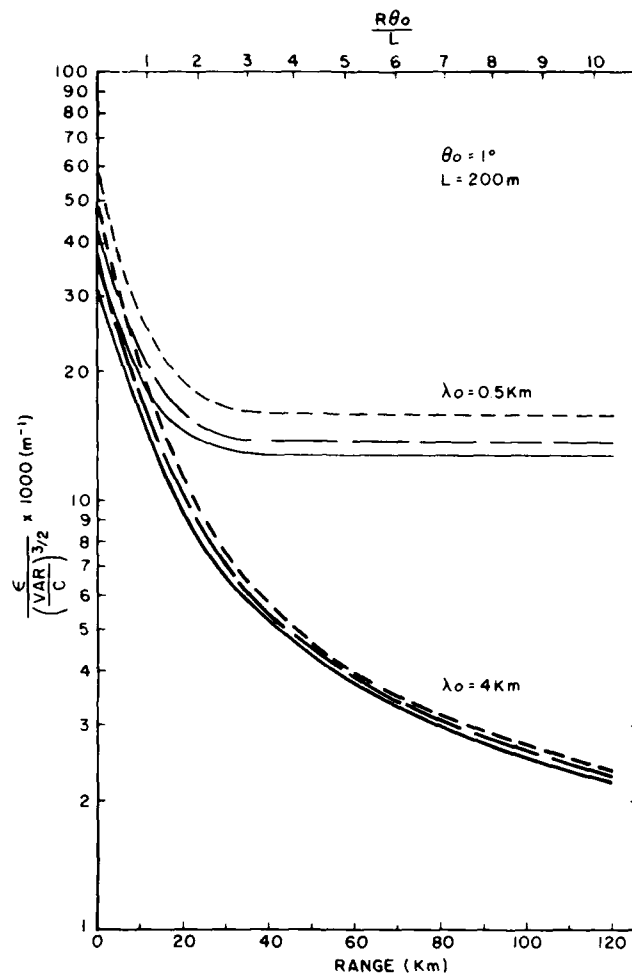
If only spectrum variance data is available, then observation of the variation of Doppler spectrum variance with range (as in Figure 5b) may identify a reasonable outer scale, thus allowing for estimation of the eddy dissipation rate. In vigorous storms, such as thunderstorms, such a technique may not be feasible. Furthermore, because of the storm structure, power spectrum analysis of the Doppler mean for the purpose of estimating the turbulence outer scale may be of little use. For such cases, it may be possible to establish a generic turbulence outer scale (sort of a mean storm value) perhaps distinguished by storm structure, maximum equivalent reflectivity factor, or other observable storm feature, which will allow for important conclusions concerning turbulence intensity to be drawn. This concept is supported by Doviak et al.[11] who indicate that the variance of the Doppler spectrum does not increase dramatically with range for storm ranges of 50 to 120 km. This suggests, after comparison with Figures 5a and 5b, that turbulence may frequently be the major contribution to Doppler spectrum variance, and that on the average the turbulence outer scale may be 1 to 3 km. This result would be in agreement with general aircraft observations.

Consider the following exaggerated example. An outer scale length of 2 km is assumed in an environment where λ_o actually varies from 1 to 4 km. The Doppler spectrum variance is allowed the two extreme values of 1 and 36 m^2/sec^2. Table 1 outlines the estimated eddy dissipation rate values ($\varepsilon^{1/3}$), a quantity typically used as a turbulence severity indicator. In each case the severity estimate derived from the generic turbulence outer scale value estimates well the two true possible turbulence intensities. Thus, use of a reasonable estimate of turbulence outer scale may allow for accurate classification of turbulence severity when only Doppler spectrum variance information is available. For ranges greater than about 20 km, such a method would always be superior to the commonly used relation of Frisch and Clifford,[10] which as observed in Figure 6a, will always underestimate the eddy dissipation rate.

Finally, it must be realized that all the results derived here have been for a particular hypothetical radar having a pulse volume depth of 200 m and full half-power beamwidth of 1°. Variations in pulse volume depth should noticeably modify the results in only those situations where pulse volume depth is the largest pulse volume dimension. Figure 7 displays the ratio ($\varepsilon_{100}/\varepsilon_{200}$) of normalized eddy dissipation rate from two radars having the same 1° beamwidth, but differing pulse volume lengths of 100 and 200 m. Perfect tracers were assumed; however, the conclusions are applicable to all precipitation environments considered here. Note that $\varepsilon_{200} = \varepsilon/(\langle VAR \rangle /C)^{3/2}$ and for $\lambda_o = 1$ km would simply be the $\lambda_o = 1$ km

11. Doviak, R.J., Sirmans, D., Zrnic, D., and Walker, C.R. (1978) Considerations for pulse Doppler radar observations of severe thunderstorms, J. Appl. Meteor. 17:189-205.

Table 1. Turbulence Intensity Estimate $\epsilon^{1/3} \, cm^{2/3} \, sec^{-1}$

Turbulence Intensity Estimate $\epsilon^{1/3} \, cm^{2/3} \, sec^{-1}$					
	Range = 40 km	Range = 120 km	Outer Scale (km)	Intensity Scale[12]	
$\langle VAR \rangle = 1 \, m^2 \, sec^{-2}$	3.8	1.7	1	<0.6	negligible
	3.4	1.3	2	0.6-1.5	light
	3.3	1.2	4	1.5-3.5	moderate
				3.5-8.2	heavy
$\langle VAR \rangle = 36 \, m^2 \, sec^{-2}$	10.7	10.0	1	>8.2	severe
	9.6	8.0	2		
	9.2	6.9	4		

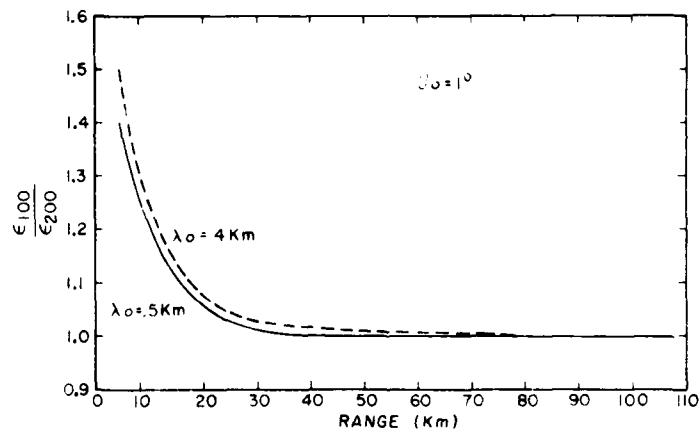Figure 7. Ratio of Normalized Eddy Dissipation Rate $\epsilon/(\langle VAR \rangle/C)^{3/2}$ for Two Radars Having 100 and 200 m Pulse Volume Depths. Full half-power beamwidth is 1°. Turbulent outer scale is $\lambda_o = 0.5, \, 4$ km

12. MacCready, P. (1964) Standarization of gustiness values from aircraft, J. Appl. Meteor. 3:439-449.

curve in Figure 6a. Thus ϵ_{100} is the equivalent curve for a radar having a 100 m pulse volume depth. A ratio of 1 at some range means that the two curves would be colocated at that range and both radars would measure the same Doppler spectrum variance and eddy dissipation rate. A ratio of 1 for all ranges means the curves for the two radars would be identical. The plot indicates significant difference only for ranges less than about 10 km. Thus, the curves presented in Figures 5 and 6 should be applicable to 1^O beamwidth radars at ranges greater than about 20 km and having typical pulse volume depths of 100 to 300 m. Additionally, a change of 10 to 20 percent in beamwidth would probably result in a similar change in measured Doppler spectrum variance. The resulting change in $\epsilon^{1/3}$ (proportional to $\langle VAR \rangle^{1/2}$) should be much less. Thus the results presented here should be applicable to most meteorological radars of similar dimensions.

3. AIRCRAFT AND RADAR DATA ANALYSES

The material presented so far deals with the contribution to Doppler spectrum variance from precipitation in a given turbulent environment. This variance has been shown to be directly dependent upon the two basic turbulence parameters. The eddy dissipation rate is the quantity of interest since it describes the intensity of turbulent air motions in the wind field. However, Figures 5 and 6 demonstrate that some knowledge of the turbulence outer scale is required before we can successfully estimate this quantity. It was stated that turbulence in thunderstorms may be localized; there are a few patches wherein the turbulence is roughly homogeneous. The following material shows results of first analyses of aircraft thunderstorm gust velocity data which appear to support this concept and yield estimates of both ϵ and λ_0.

The following data were acquired on May 26, 1976 by an Air Force F-4 instrumented aircraft. Two penetrations, separated by approximately 30 minutes, were made at a height of about 16,000 ft (4876.8 m) through a portion of a storm complex located 40 km south of Norman, Oklahoma. Aircraft measurements were taken every 0.1 second. The first run (run 1) was from 210°. The second run (run 2) passed through roughly the same storm region, but from 80° and 30 minutes later. Aircraft speed was at 198 m/sec during both runs. The discussion will center around the analysis of the vertical gust velocity data.

Figures 8 (a through e) and 9 (a through e) are plots of the vertical gust velocity, derived gust velocity, environmental temperature, aircraft normal acceleration, and barometric altitude during the two runs. The prominent feature in run 1 is the apparent strong upward-moving current between 52510 and 52540. It is about 6 km wide and is characterized by a warmer temperature than the environment
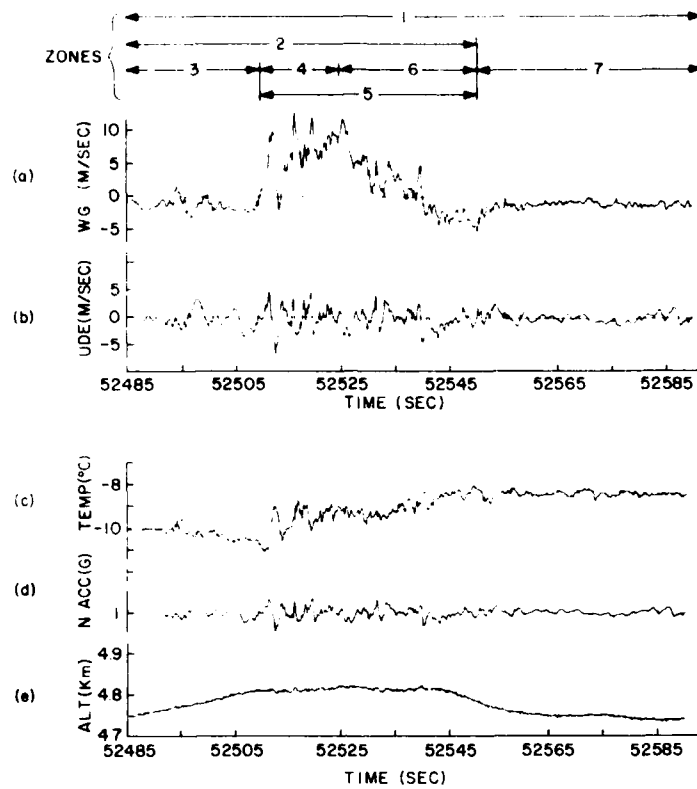
33

Figure 8. Aircraft Time Series Data for Early Aircraft Run
of (a) Vertical Gust Velocity, (b) Derived Gust Velocity,
(c) Environmental Temperature, (d) Normal Acceleration,
(e) Barometric Altitude. Analyzed segments are labeled 1
through 7

during entry and increased normal acceleration of the aircraft. Also note the large
spikes in the vertical gust velocity of a somewhat periodic nature, suggesting the
possible presence of waves. Similarly, run 2 exhibits two apparent upward-moving
air currents centered at 53775 and 53910 sec respectively. The period 53555
through 53645 exhibits strong periodic fluctuations. Increased aircraft normal
acceleration and spikes in vertical gust velocity are also noticed here.

Casual observation of these two plots suggests that each gust velocity time
sequence may be segmented into a number of discrete local turbulence zones. In
run 1, we focus on three zones labeled 3, 5, and 7 in Figure 8, part (a), corre-
sponding to the visually estimated turbulence classes moderate, heavy within
updraft region, and light, respectively. Similarly, in run 2 (Figure 9, part
(a)), the time series is segmented into zones 1, 5, 6, 9, 7, and 8 respectively.
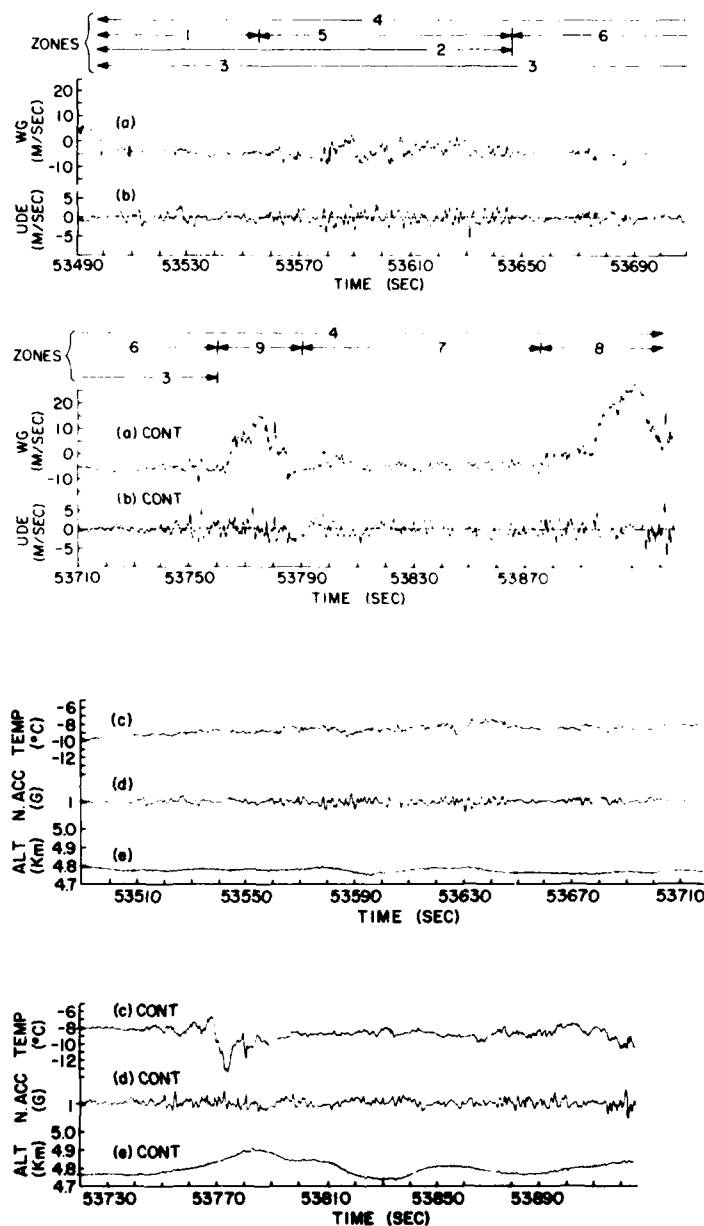
34

Figure 9. Aircraft Time Series Data for Late Aircraft Run
of (a) Vertical Gust Velocity, (b) Derived Gust Velocity,
(c) Environmental Temperature, (d) Normal Acceleration,
(e) Barometric Altitude. Analyzed segments are labeled 1
through 9

35

Each gust velocity time series was subjected to power spectral analysis (PSA). The analyses were conducted on segments of the original data sets. Segments consisted of one or more of the individual zones and are labeled 1 through 7 (run 1, Figure 8) and 1 through 9 (run 2, Figure 9) respectively. Each segment was linearly detrended before being subjected to spectrum analysis. Although detrending forces the power spectral density to go to zero at zero frequency, the spectral outer scales are generally well beyond the influence of this scale removal action, and should represent a true change of spectral slope. Figures 10 and 11 show the power spectral density (PSD) plotted as a function of radian frequency. An approximate space scale is also included. Observations from run 1 will be presented first.

It is observed that the spectra may be calssified according to where the sharp changes in slope (knee) of the curves occur. Spectra c, d, and f exhibit apparent slope changes at scales less than 1 km, whereas spectra a, b, e, and g appear to have the knee located at scales greater than 2 km. It is believed that segment 7 (spectrum g) would also have shown a small outer scale length if the time record 52550 through 52555 had not been included. Reference to Figure 8 part (a) shows that spectra a, b, and e are strongly biased by inclusion of the upcurrent region as a turbulent fluctuation rather than as a true feature of the larger storm wind structure. The updraft region thus acts as a large, very energetic eddy which strongly biases the strength (V^2) of the turbulent field and introduces extra energy into the long wavelength region of the PSD curves. In the sense that the upcurrent does not qualify as a truly turbulent feature, it is inappropriate to blithely include it in PSA. Spectra d and f show the power spectra derived from the fluctuations imbedded in the positive and negative slope portions of this upcurrent region. It is seen that these spectra are similar to spectrum c. Referring back to Figure 4b, it is observed that the knee of the spectral curve well represented the turbulence outer scale length under the ideal conditions of homogeneous isotropic turbulence. It is felt that here the knee may be a reasonable measure of this parameter.

Now consider run 2. These spectra are not as easily categorized. It is clear that segment 4, which includes all data as turbulence, exhibits the largest apparent outer scale value and generates large spectral densities at long wavelengths. Again, this results from inclusion of the updraft features as turbulent gusts. The lower power but prominent peak near .08 km in spectrum a results from a 0.5 sec ripple riding on the gust velocity trace. These fluctuations are too fine to be seen in these highly reduced traces. In spectrum f a long (approximately 40 sec) modulation is the likely cause of the spectral peak near 4.6 km. It is instructive to compare spectra a, c, e, and f. Note that spectra a, e, and f have a well defined knee. However, when these three regions are combined into one (3), the resulting spectrum does not exhibit this clear slope change at short scales. In this instance,
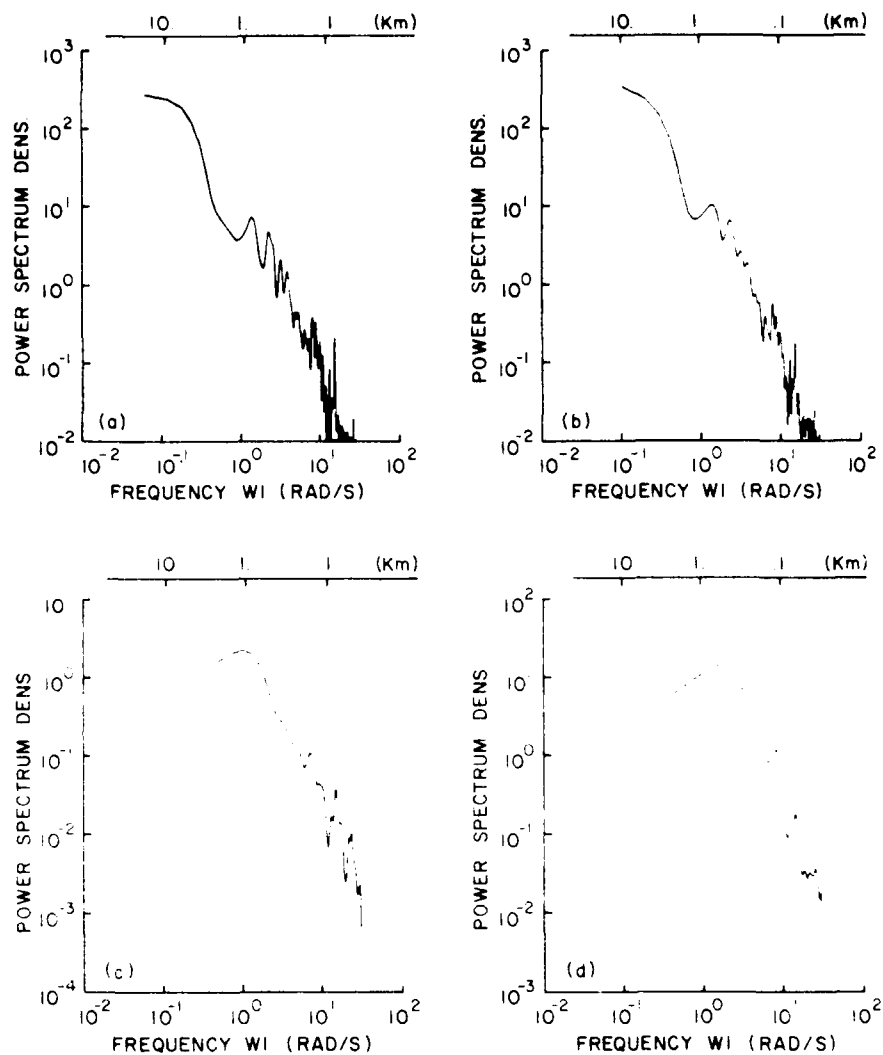
36

Figure 10. Turbulence Power Density (m^2/sec^3) Versus Frequency (rad/sec) for Segments 1 through 7 in Figure 8. Part (a) corresponds to segment 1, (b) to segment 2, etc. Apparent space scale at top

Figure 10. Turbulence Power Density (m^2/sec^3) Versus Frequency (rad/sec) for Segments 1 through 7 in Figure 8. Part (a) corresponds to segment 1, (b) to segment 2, etc. Apparent space scale at top (Continued)
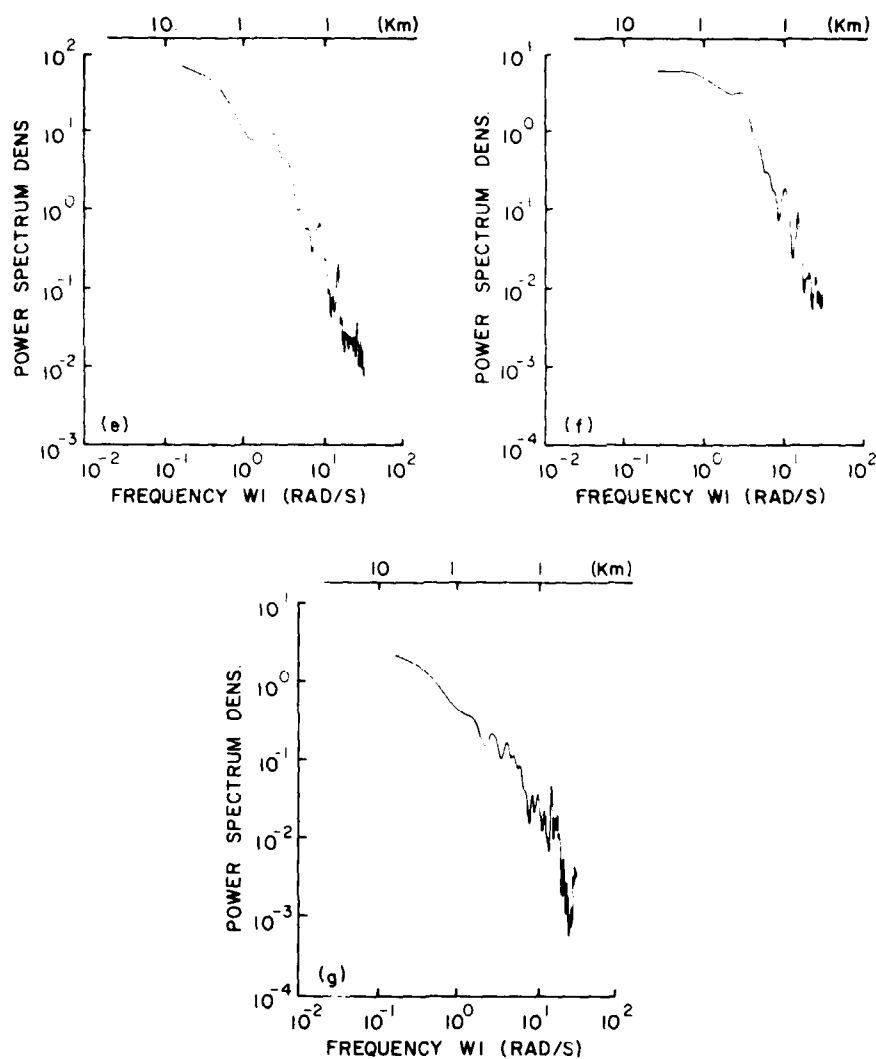
38

Figure 11. Turbulence Power Density (m^2/sec^3) Versus Frequency (rad/sec) for Segments 1 through 8 in Figure 9. Part (a) corresponds to segment 1, (b) to segment 2, etc. Apparent space scale at top

39

Figure 11.   Turbulence Power Density (m^2/sec^3) Versus Frequency (rad/sec) for Segments 1 through 8 in Figure 9.   Part (a) corresponds to segment 1, (b) to segment 2, etc.   Apparent space scale at top (Continued)
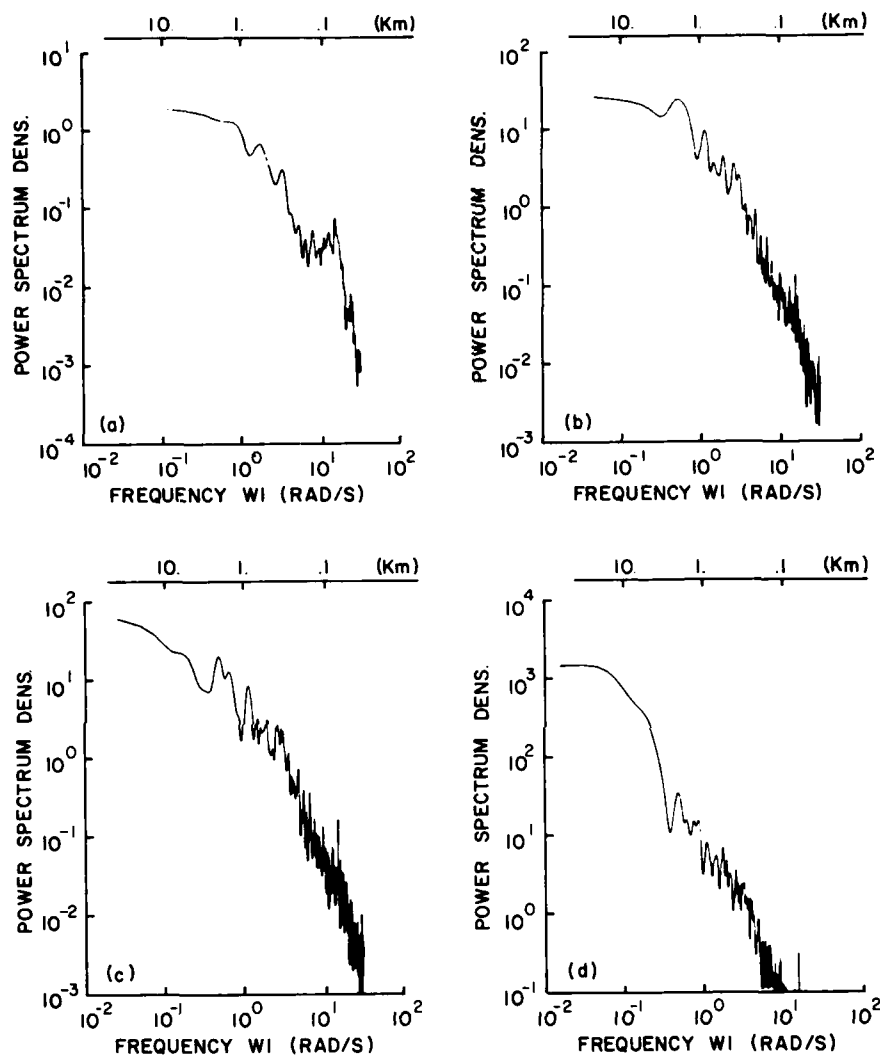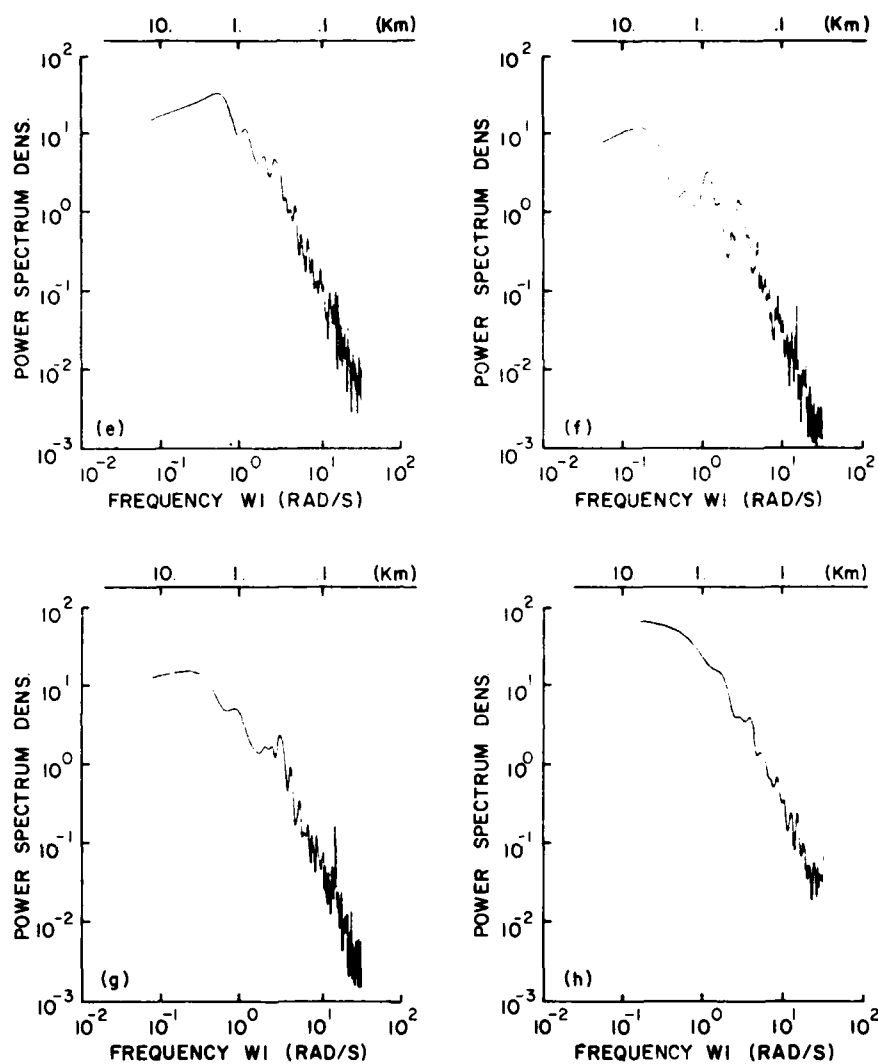
segment 5 appears to act similarly to an upcurrent region for the composite segment. The apparent turbulence outer scales for run 2 for the individual segments are in the range .4 to 2.4 km. These data indicate that inclusion of storm structure, nonturbulent fluctuations, and composites of local turbulent patches can strongly influence the resulting apparent turbulent power spectra derived from the data.

Table 2 provides the mean square velocity, estimated outer scale length, and estimated eddy dissipation rate for these various spectra. Note that the outer scale lengths are considerably larger for run 2 than for run 1. This difference may be a result of sampling nonidentical storm regions, but may also indicate a temporal evolution. The almost synergistic effect of combining local turbulence zones into single larger units is dramatically demonstrated by the air motion variance V^2. Surprisingly, the eddy dissipation rates for the individual zones of the two spectral sets are very similar. Within nonupdraft regions, both runs show ε in the range 13 to 360 cm^2 sec^{-3}. The largest ε are found within the updraft regions and range from 490 to 1665 cm^2 sec^{-3}. These values indicate that nonupdraft regions would be characterized as moderate in strength, while the updraft regions are heavy to extreme.[12]

Table 2. Estimated Turbulence Parameters

Spectrum Segment No.	1	2	3	4	5	6	7	8
$V^2(m^2/s^2)$	12.19	17.73	0.77	7.56	9.25	2.81	0.41	(Early Period)
λ_o(km)	0.62	0.62	0.95	0.5	4	0.38		
$\varepsilon(cm^2/sec^3)$	2749	4823	29	1665	282	490		
$V^2(m^2/sec^2)$	0.534	4.15	3.34	32.36	5.84	1.33	2.39	12.38 (Late Period)
λ_o(km)	1.18	1.8	2.48		2	1.13	0.41	2.06
$\varepsilon(cm^2/sec^3)$	13	188	99		283	54	360	847

Finally, it is instructive to correlate the aircraft and radar data to determine if the radar is properly measuring the turbulent contribution to Doppler spectrum variance. This must be ensured before radar variance data are interpreted in terms of turbulent field parameters. Before presenting the results in detail,

41

however, the radar data and the techniques applied to the radar and aircraft data to prepare them for the correlation analysis will be described.

The radar data were interpolated onto a Cartesian (x, y, z) grid. The horizontal surfaces were separated vertically by $\Delta z = 0.5$ km. The grid point separation within the surfaces was also $\Delta x = \Delta y = 0.5$ km. A horizontal surface near 4 km agl represents the surface through which the aircraft flew and radar data fields for this level will be shown. The Doppler spectrum variances were obtained by use of the Fast Fourier Transform on original complex time series radar data. The Doppler spectra were then analyzed using an objective thresholding scheme which automatically determined the spectrum noise level, isolating the true meteorological signal from which the spectral mean and variance were determined.

Figures 12 and 13 show the equivalent reflectivity factor Z_e (dBZ) for the early and late aircraft runs, respectively. The storm was propagating towards the NE in both cases. The portions of the aircraft track that were eventually found to be best correlated with the radar data are shown. In the early run (Figure 12) the aircraft flew through one cell which had a $Z_e > 36$ dBZ, and was part of a storm complex. The actual length of aircraft track also observed by radar is about 11 km in length and is shown by the line segment in this plot. The late period (Figure 13) shows the aircraft flew through a storm consisting of one large storm cell of $Z_e > 36$ dBZ. The corresponding aircraft track supported by radar data is about 38 km long. The maximum Z_e (<40 dBZ) values in both storms are not indicative of severe weather; however, the cells are strong enough to require normal avoidance by aircraft. Figures 8, part (a) and 9, part (a) indicate that the aircraft flew through at least one updraft region in each run. With only one radar scanning nearly horizontally, actual vertical velocities cannot be measured. However, information from plots of radar radial velocity, shown in Figures 14 and 15, when combined with the Z_e plots do suggest the updraft positions.

Since the storms were moving NE, the Z_e cells would normally be expected to lie just upwind (SW) of their associated updrafts. Updrafts in horizontal radial velocity plots generally appear as regions having a magnitude near zero. Both radial velocity plots show regions of marked decrease of radial velocity magnitude in the vicinity of the high Z_e cells penetrated by the aircraft. In the late period the aircraft penetrated the southern end of a velocity minimum, which is suggestive of an updraft region. In the early period, the aircraft penetrated a broad region of marked decreased magnitude, but not a well defined minimum. These regions agree well with the aircraft updraft positioning (shown as U in Figures 14 and 15) determined by the aircraft track.

Because we are primarily interested in the turbulent contribution to Doppler spectrum variance and wish to correlate the radar and aircraft Doppler spectrum variance estimates, other factors which broaden the radar variance estimates
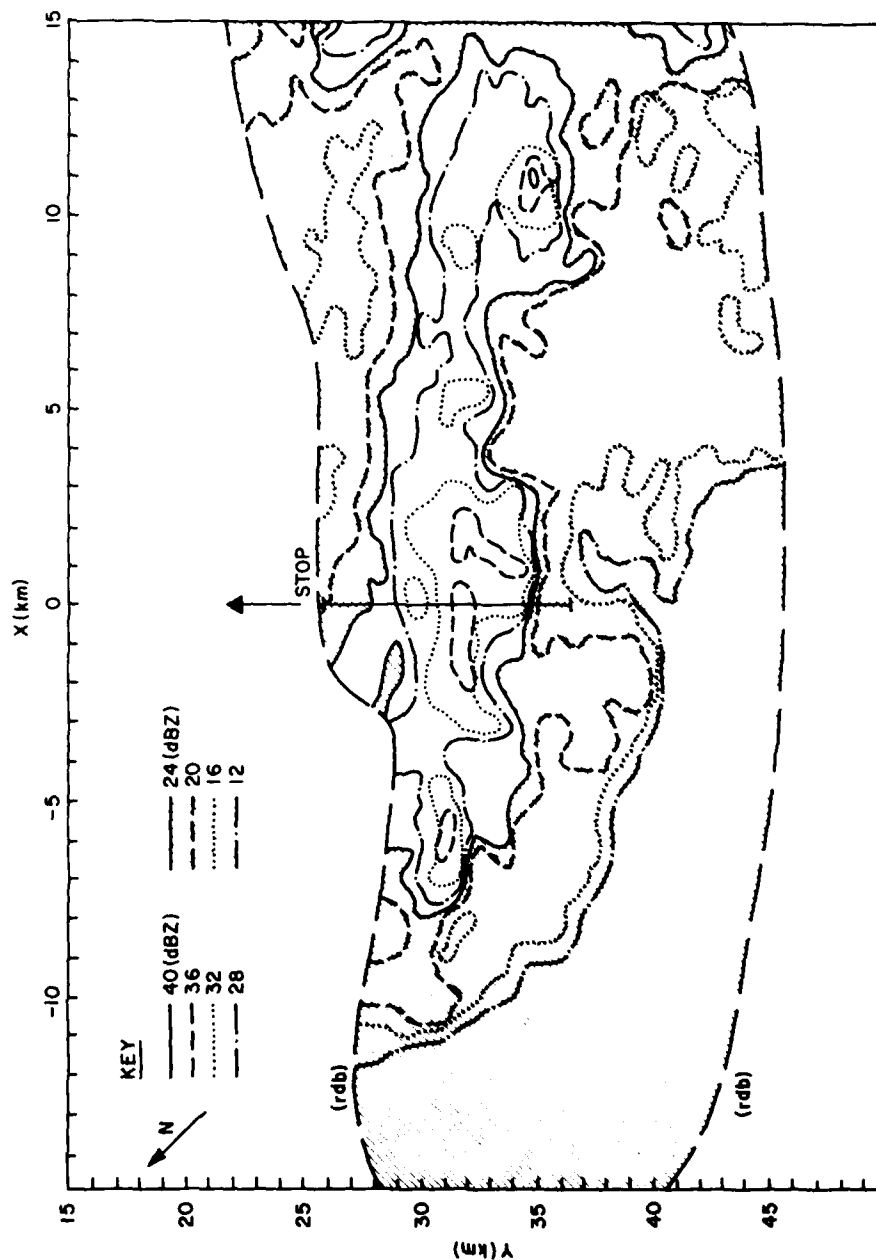
42

Figure 12. *Radar Equivalent Reflectivity Factory* Z_e *(dBZ) on Horizontal (x, y) Surface at 4 km agl During Early Aircraft Run.* Segment of aircraft time series correlated with radar data shown by line segment. Radar is at (0, 0) and rdb is radar detectable *boundary*
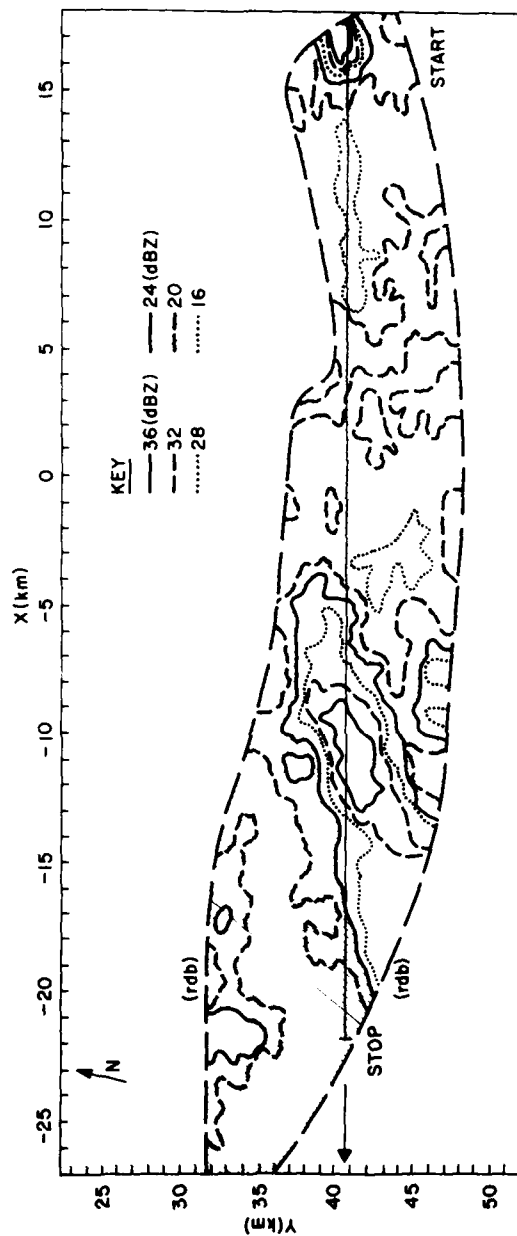
43

Figure 13. Radar Equivalent Reflectivity Factory Z_e (dBZ) on Horizontal (x, y) Surface at 4 km agl During Late Aircraft Run. Segment of aircraft time series correlated with radar data shown by line segment. Radar is at (0, 0)
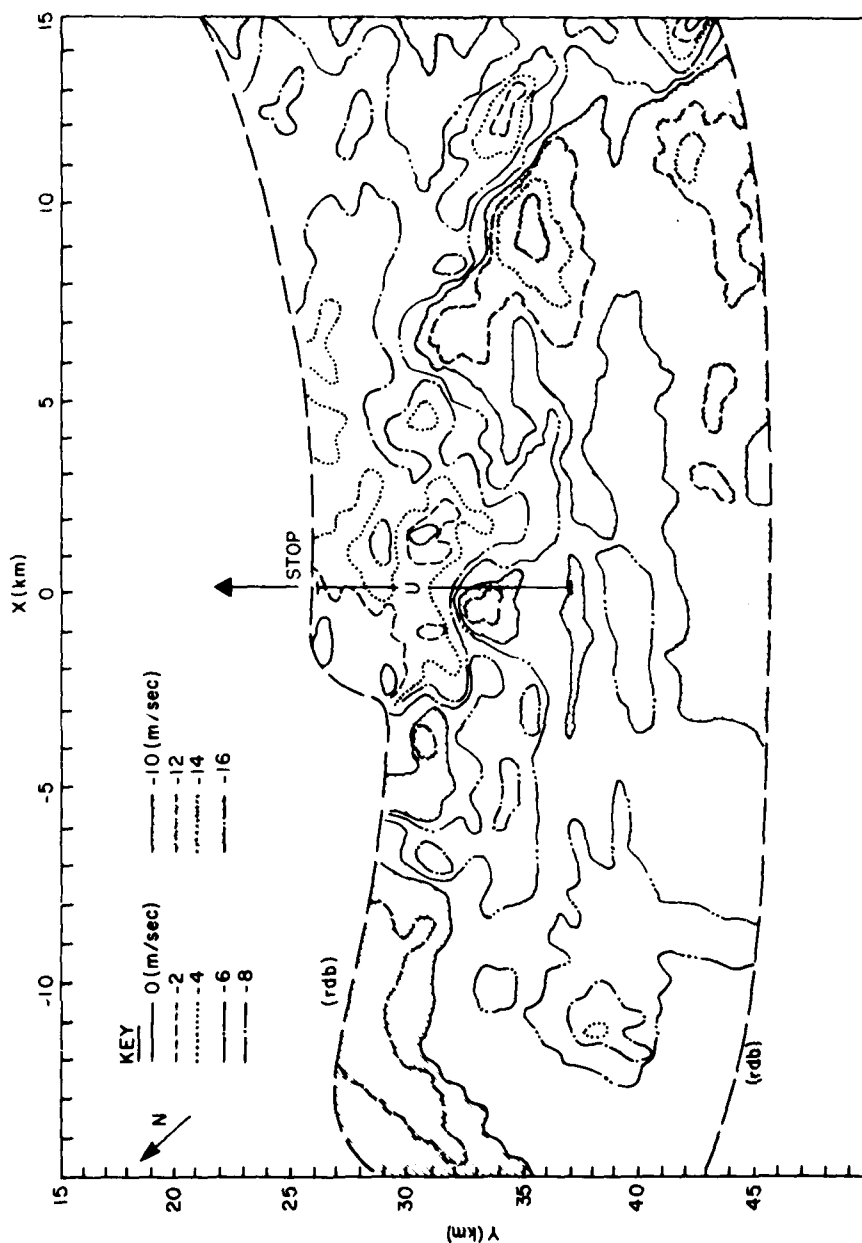
44

Figure 14. Radar Radial Velocity (m/sec) on Horizontal (x, y) Surface at 4 km agl During Early Aircraft Run. U is the aircraft estimated updraft location
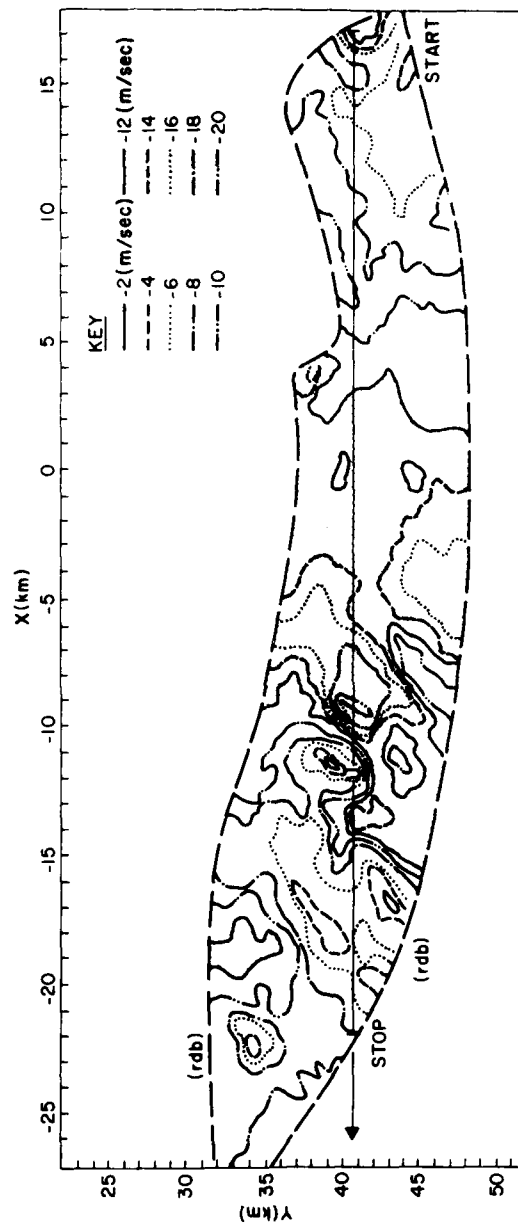
Figure 15. Radar Radial Velocity (m/sec) on Horizontal (x, y) Surface at 4 km agl During Late Aircraft Run. U is the aircraft estimated updraft location

must be removed. At the low elevation angles scanned ($<8^{\circ}$), the only significant contributors other than turbulence are the transverse shears of the radial wind. These were estimated over the level of aircraft flight and are shown in Figures 16 and 17, and Figures 18 and 19, for the early and late periods respectively.

The vertical shear of the radial wind for the early period shows maximum shear values of about 7×10^{-3} sec^{-1}. Curiously, the only Z_e cell which does not show a shear maximum in close proximity is the cell penetrated by the aircraft. Because of the spectral processing techniques applied, large transverse shear values found outside vigorous storm regions may generally be considered representative of the environmental wind and not simply a result of low spectrum power. The horizontal shear of radial velocity plot (Figure 17) shows a markedly periodic pattern of positive and negative shear maxima through the entire region of moderate storm intensity ($Z_e > 24$ dBZ). The structure has a spacing of about 3 km per maximum. Considering each adjacent pair as a single unit (for example, each pair could represent a circulation, or vortex eddy) suggests that the storm complex has a basic small scale structure of about 6 km. This scale is much larger than the 0.5 km grid spacing and probably represents the dominant structure scale in the storms.

For the late period the vertical shear also has a maximum value of about 7×10^{-3} sec^{-1}. Also, although the most significant shear is colocated with the single large Z_e cell, strong vertical shear is again observed outside the storm cell. The horizontal shear shows the pattern of positive and negative maxima, although not as vividly as in the early period. The small scale storm structure here is closer to 7 km in size. The shear estimates displayed in Figures 16 through 19 were used to compute the shear contribution to Doppler spectrum variance. These contributions were then subtracted from the Doppler spectrum variance values, resulting in variance estimates which were dominated by turbulent contributions.

The turbulence produced Doppler spectrum variance estimates are shown in Figures 20 and 21. The early period (Figure 20) shows that the variance is generally <6 m^2 sec^{-2} outside the storm ($Z_e < 20$ dBZ) and usually closer to 2 m^2 sec^{-2}. The high Z_e cells within the storm complex exhibit variance >4 m^2 sec^{-2} and are generally closer to 8 m^2 sec^{-2}. Within the storm complex in general (20 dBZ $< Z_e < 36$ dBZ) the variance values are in the range 2 to 6 m^2 sec^{-2}. The late period (Figure 21) similarly shows spectrum variance to be <4 m^2 sec^{-2} outside the storm (<20 dBZ), >8 m^2 sec^{-2} within the high Z_e cell, and 2 to 6 m^2 sec^{-2} elsewhere in the storm.

As with any general rule there are exceptions. Good examples where large Doppler spectral variance exists outside high Z_e cells are seen at (-4, 35) in Figure 20, and (-22, 33) and (-2, 47) in Figure 21. Noting that large variance
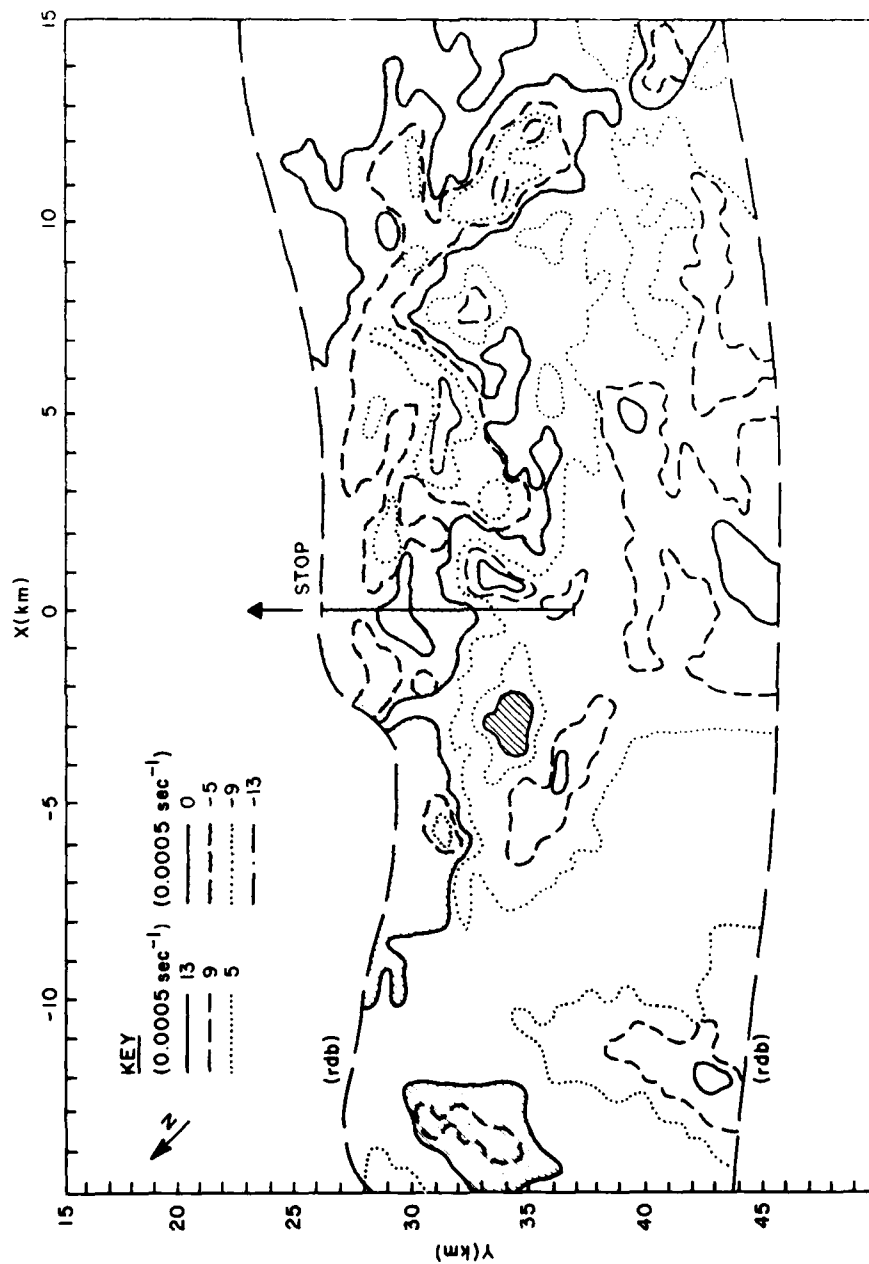
47

Figure 16. Vertical Shear of Radial Velocity (Units of 0.0005 sec^{-1}) on Horizontal (x, y) Surface at 4 km agl During Early Aircraft Run
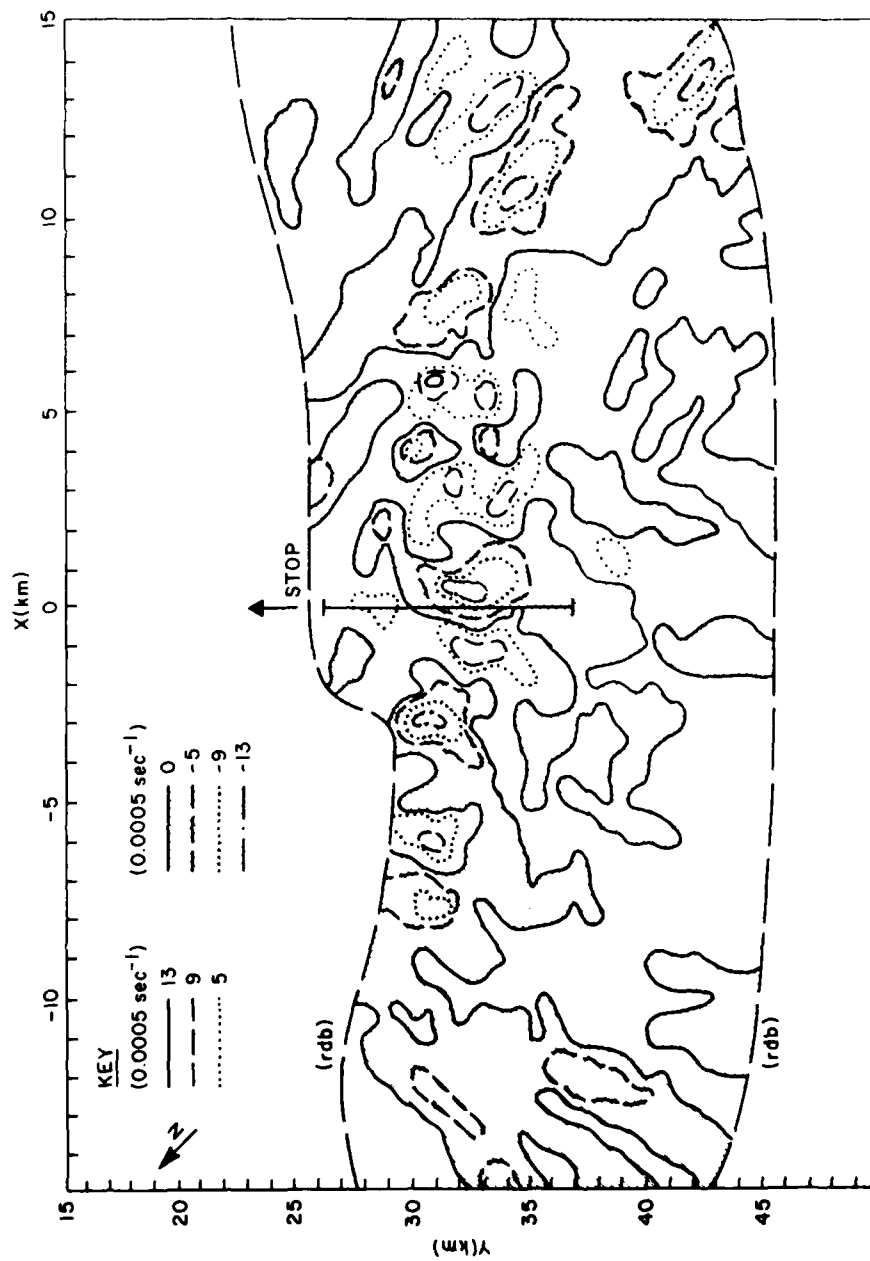
Figure 17. Horizontal Shear of Radial Velocity (Units of 0.0005 sec⁻¹) on Horizontal (x, y) Surface at 4 km agl During Early Aircraft Run

Figure 18. Vertical Shear of Radial Velocity (Units of 0.0005 sec^{-1}) on Horizontal (x, y) Surface at 4 km agl During Late Aircraft Run

KEY
9 (0.0005 sec^{-1})
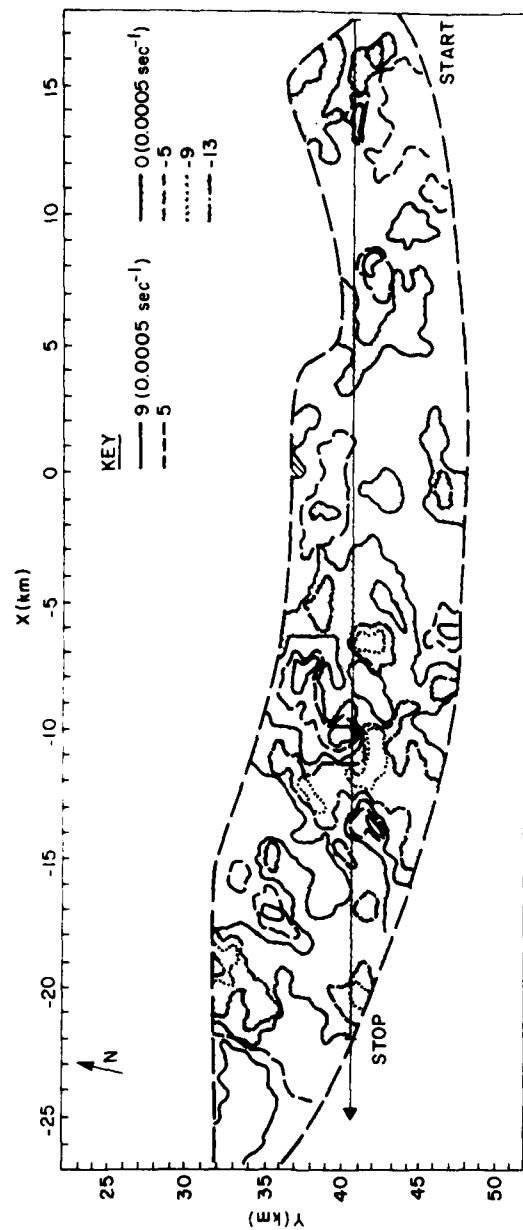5
0 (0.0005 sec^{-1})
-5
-9
-13

50

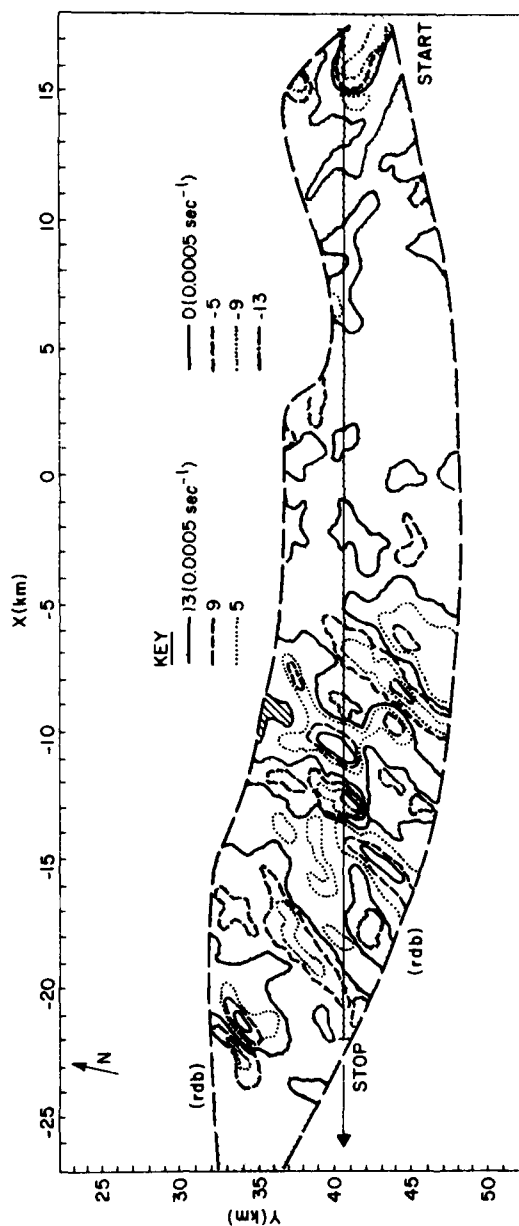Figure 19. Horizontal Shear of Radial Velocity (Units of 0.0005 sec^{-1}) on Horizontal (x, y) Surface at 4 km agl During Late Aircraft Run
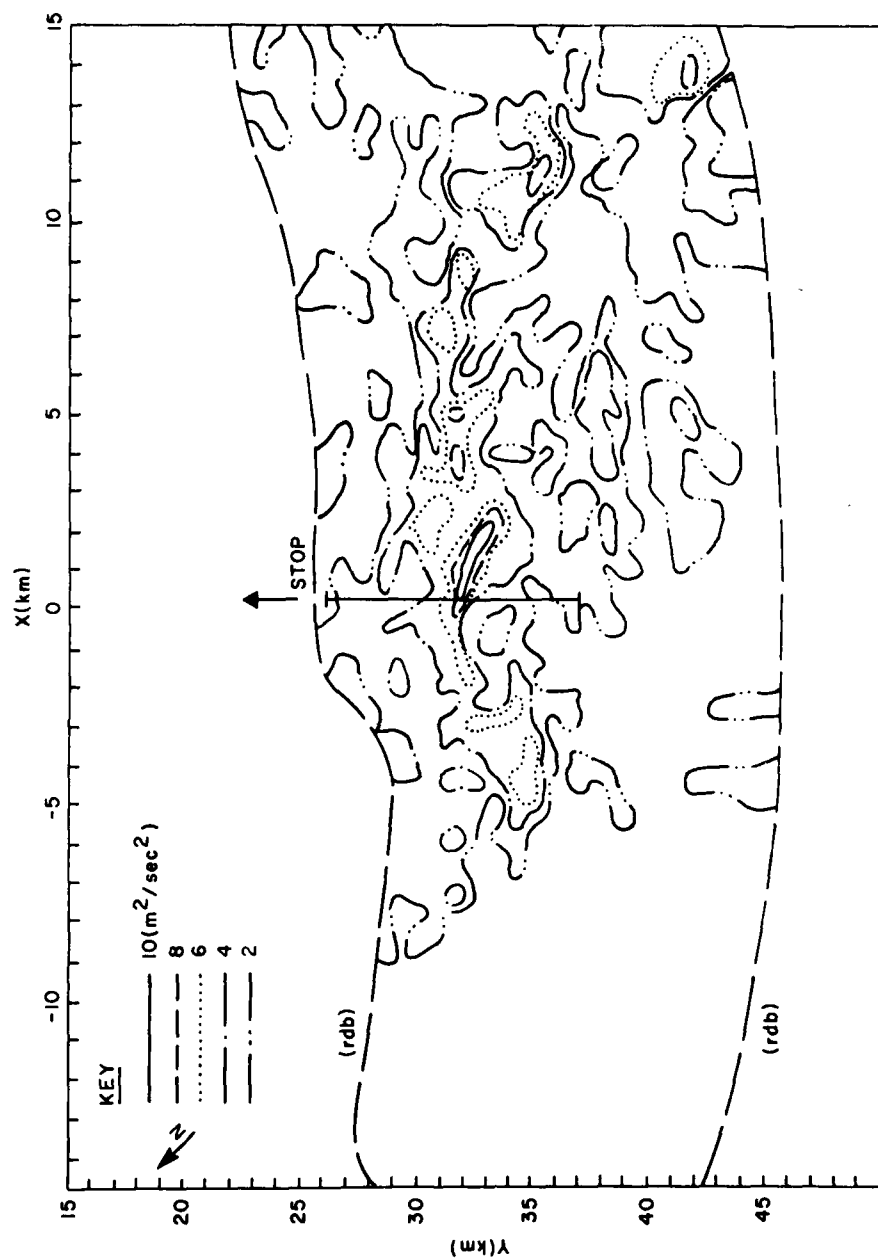
51

Figure 20. Turbulence Induced Doppler Spectrum Variance (m^2/sec^2) on Horizontal (x, y) Surface at 4 km agl During Early Aircraft Run
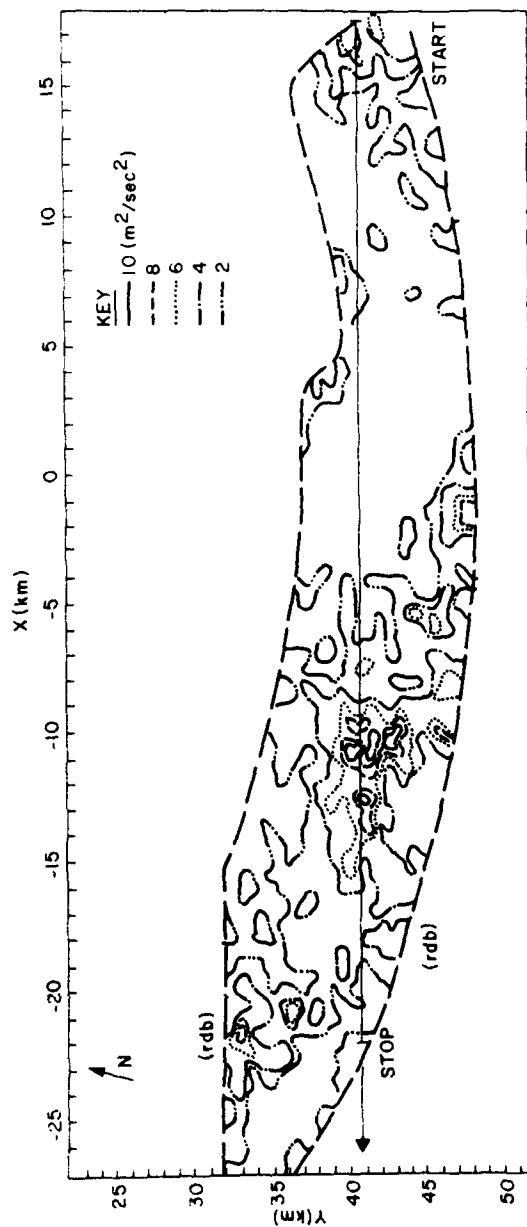
Figure 21. Turbulence Induced Doppler Spectrum Variance (m^2/sec^2) on Horizontal (x, y) Surface at 4 km agl During Late Aircraft Run

generally represents energetic turbulent conditions (Figure 6), we see that these failures show that hazardous zones may frequently be found outside high Z_e cells and outside what one would generally consider the outer storm boundary. Next we return to the task of comparing these radar spectrum variance estimates with the equivalent aircraft derived values.

The aircraft gust velocity data consist of a time series of vertical gust components separated in distance by about 0.02 km. To obtain equivalent Doppler spectrum variance estimates from aircraft data the following procedure was followed. First, a continuous time series of gust velocity components was formed by taking the individual detrended segments (3, 4, 6, and 7 for the early run [Figure 8]; and 1, 5, 6, 9, 7 and 8 for the late run [Figure 9]) and coupling them to form a single time series of "true" gust velocity. These series are shown in Figures 22 and 23. Second, a Gaussian filter representing the radar beam pattern function was applied to each time series to obtain a time series of equivalent Doppler spectrum variance for each run. These variance estimates are thus estimates of what the radar would have measured if it observed these aircraft vertical gust velocity components in a field of uniform reflectivity. Next, to correlate this data set with the actual radar variance data shown in Figures 20 and 21, the aircraft data were interpolated to a set of grid points along the aircraft track. The grid points were separated by 0.5 km. This technique results in aircraft and radar data which have undergone similar beam filtering and interpolation to Cartesian grid locations.

Before proceeding further, however, we must take note of deficiencies in this method. First, the aircraft equivalent variance is derived from the vertical turbulent gust velocity while the radar spectrum variance is derived from essentially the horizontal component of turbulent gust velocity. Second, for the aircraft measurement the radar beam pattern function was applied to a line of aircraft data, but to a volume defined by the radar pulse volume for the radar measurement.
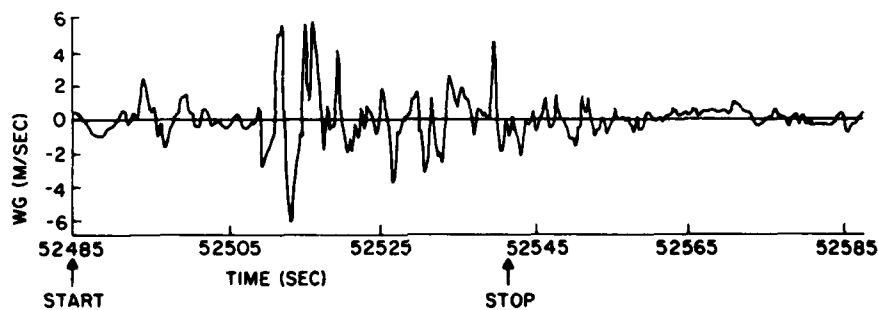

Figure 22. Time Series of "True" Vertical Gust Velocity for Early Aircraft Run
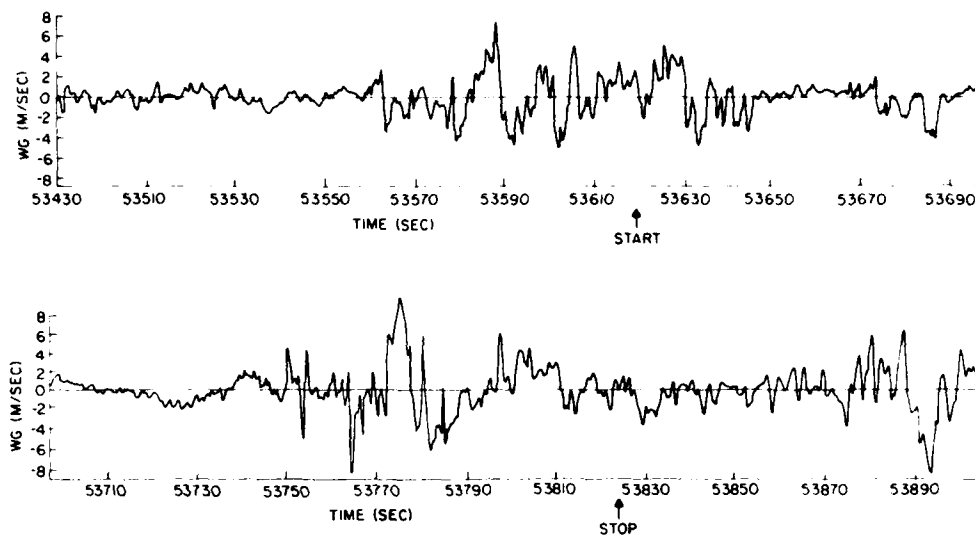
54

Figure 23.   Time Series of "True" Vertical Gust Velocity for Late Aircraft Run

Also note that use of a 0.5 km grid point system introduces error since radar data can be interpolated to a grid point from regions through which the aircraft did not fly. One is forced to use some sort of grid system, however, since the aircraft position actually fluctuates off the mean flight path by hundreds of meters. Last, because the radar was not slaved to the aircraft location, temporal evolution of turbulent fields between the times when the radar and aircraft sampled the same general region could have occurred. Thus, differences between the radar and aircraft Doppler spectral estimates are not unexpected.

The best correlated Doppler spectrum variance data sets for aircraft and radar are shown in Figures 24 and 25. The early data set (Figure 24) has a correlation coefficient of 0.891 and the late period (Figure 25) has a correlation coefficient of 0.821. Considering the deficiencies of the technique mentioned above, the degree of correlation is quite remarkable and suggests that the sampled turbulent fields may be nearly isotropic. In both plots the region of largest spectrum variance is in best agreement, suggesting that conditions approaching isotropicity are more likely in regions of strong turbulence than in regions of light turbulence. The fact that these data correlate well suggest that turbulence parameters determined from the radar data alone may generally estimate well the actual environmental values. Last, it is noteworthy that the minimum radar variance is generally about $2 \, m^2 \, sec^{-2}$ while the corresponding aircraft values are closer to $0.25 \, m^2 \, sec^{-2}$. This may result from deficiencies in the technique mentioned above, or indicate

55

Figure 24. Plots of Radar (Solid Line) and Aircraft (Dotted Line) Estimates of Doppler Spectrum Variance at Grid Points Along Aircraft Track, for Early Aircraft Run. Abscissa is distance (km) along correlated portion of aircraft track
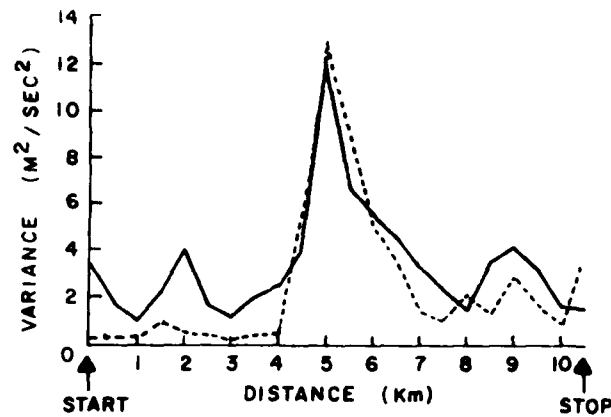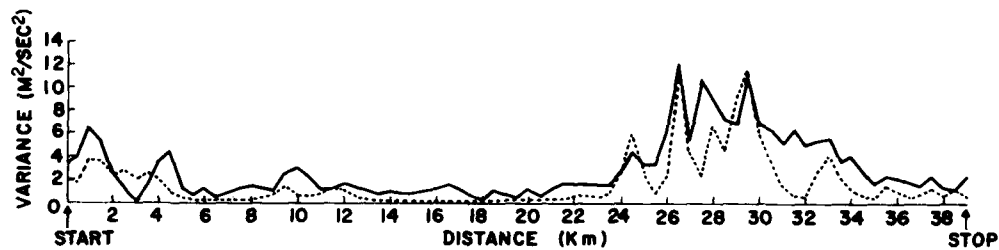

Figure 25. Plots of Radar (Solid Line) and Aircraft (Dotted Line) Estimates of Doppler Spectrum Variance at Grid Points Along Aircraft Track, for Late Aircraft Run. Abscissa is distance (km) along correlated portion of aircraft track

that additional noise or small scale storm structure may still be contaminating the radar data.

It is unclear whether the discrepancies in these variance plots result from deficiencies in the technique as noted above, or from an incomplete understanding of how the turbulent precipitation motions are mapped into Doppler spectrum variance. It is also unclear whether the agreement seen here would be retained on a radar pulse volume scale, rather than the 0.5 km grid scale employed. To answer

56

these questions, more complete data sets where the aircraft measures all three gust velocity components and where the radar pulse volume is slaved to the aircraft location are required.

The results discussed here will allow for increased accuracy in Doppler radar estimation of turbulence intensity, and will have practical application. As stated earlier, the two main contributions to Doppler spectrum variance are the transverse shear of the radial wind and turbulence. The Doppler radar can estimate the shear component by observing the variation in azimuth and elevation of the mean Doppler velocity between successive radials. Thus, the turbulent contribution can be estimated. With some knowledge of the turbulence outer scale and storm reflectivity factor, a reasonable estimate of the eddy dissipation rate may be obtained. This information can then be combined with the known response characteristics of aircraft for identification of regions of hazard to aircraft. Use of these results with incoherent radar is significantly more difficult, however. The incoherent radar cannot estimate the Doppler mean velocity, and therefore will not allow for the determination of the transverse shear. Thus, the turbulent variance contribution may not be well known.

Atlas and Srivastava[13] proposed a method for estimating an atmospheric structure function with incoherent radar by forming combinations of signal returns from successive pulse volumes along a given radial. They showed that the mean squared difference of Doppler velocity between the adjacent pulse volumes can be related to the Doppler spectral variances by

$$(V_2 - V_1)^2 = \frac{\lambda^2}{4} \; \frac{(P_1 + P_2)}{P_1 P_2} \; (\langle VAR \rangle_{12} (P_1 + P_2) - \langle VAR \rangle_1 P_1 - \langle VAR \rangle_2 P_2)$$

(33)

where λ is the radar wavelength, $\langle VAR \rangle_1$ and $\langle VAR \rangle_2$ are the Doppler spectral variances ($\sec^{-2}$) from pulse volume numbers 1 and 2 having total spectrum powers P_1 and P_2, and $\langle VAR \rangle_{12}$ is the variance of a composite Doppler spectrum obtained from adding the signals from the individual pulse volumes. Unfortunately, this relation produces a highly smoothed estimate of the true atmospheric structure function,[14] requiring very careful interpretation; it is also related to the environmental wind shear.

---

13. Atlas, D., and Srivastava, R.C. (1971) A method for radar turbulence detection, IEEE Trans. on Aerospace and Electronics, AES-7, No. 1, pp 179-187.

14. Sychra, J. (1974) Fluctuation Spectra and Velocity Structure Function, Tech. Rpt. 33, Lab. Atmos. Prob., U. of Chicago.

A measured Doppler radial estimate may be considered as a sum of a large-scale background wind (V_w), turbulent component (V_t), and an additional random error and noise bias (e), as

$$V = V_w + V_t + e \quad . \tag{34}$$

With this convention the left side of Eq. (33) becomes

$$(V_2 - V_1)^2 = (V_{2w} - V_{1w})^2 + (V_{2t} - V_{1t})^2 + (e_2 - e_1)^2 \tag{35}$$

where the second right hand term is actually the true Doppler estimate of the pulse volume filtered turbulence structure function. If two azimuthal pairs of pulse volumes ($[V_2, V_1]$ and $[V_3, V_2]$) are combined in this manner, then in a region where the mean turbulent air velocity over the region occupied by the pulse volumes varies little,

$$(V_3 - V_1)^2 - (V_2 - V_1)^2 \approx (V_{3w} - V_{1w})^2 - (V_{2w} - V_{1w})^2 \quad . \tag{36}$$

Using Eq. (36), a linear variation in large-scale wind can be fitted to the data, thereby providing an estimate of the large-scale shear. If a quadratic variation in the wind field is desired, two such sets of Eq. (33) may be used.

Obviously this technique is prone to error where the gradient of mean turbulent velocity is large. However, at the ranges of interest (perhaps 60 to 200 km) most of the turbulent energy is mapped into the Doppler spectrum variance. For this case, the radar estimate of the turbulent structure function is small, and its variation is not significant, allowing Eq. (36) to be useful. The validity of this relation is independent of the actual magnitude of the air turbulent intensity. Therefore, the above relations may be applicable within local patches of turbulence and may return reasonable estimates of transverse radial wind shear, thus permitting an estimate of eddy dissipation rate to be obtained. Usefulness of this technique can only be established after comparison of radial shear estimates from Doppler and incoherent techniques using real data.

4. CONCLUSIONS

The results of this theoretical investigation demonstrate that useful and understandable relationships exist between the mean and variance of Doppler spectra and turbulence in precipitation environments. It is found that Doppler spectrum variance and estimated eddy dissipation rate are strongly dependent upon the precipitation

environment for ranges less than about 20 km, and also for cases where the turbulence outer scale length is less than about 0.5 km. The Doppler spectrum variance and eddy dissipation rate are essentially independent of the turbulence outer scale length when the maximum pulse volume dimension is less than about one-half the outer scale value. As range increases, both parameters are strongly dependent upon range and outer scale length. Once the largest pulse volume dimension exceeds the outer scale length, however, Doppler spectrum variance and eddy dissipation rate are independent of range and dependent only upon the turbulence outer scale. Aircraft data analyses suggest that aircraft gust time series data should be viewed as a composite of segments of local turbulent patches wherein the turbulence parameters may be essentially constant. Agreement between aircraft and radar data support the theoretical concepts, but point to the need for more definitive data sets. While use of equivalent reflectivity factor may be sufficient to classify the precipitation environment, further investigation to determine reliable methods for remotely estimating the turbulence outer scale is needed if reasonable estimation of the turbulence eddy dissipation rate is to be accomplished. Nonetheless, good estimates of the severity of turbulence may be obtained by use of a reasonably guess of the turbulence outer scale length, and should prove useful in detecting hazardous zones within storms.

References

1. Lee, J. T. (1967) Atmospheric Turbulence and Radar Echoes in Oklahoma, Technical Memorandum IERTM-NSSL 32, Norman, Oklahoma.

2. Armstrong, G., and Donaldson Jr., R. (1969) Plan shear indicator for real-time Doppler radar identification of hazardous storm winds, J. Appl. Meteor. 8:376-383.

3. Lee, J. T., and Kraus, M. (1975) Plan shear indicator and aircraft measurements of thunderstorm turbulence; experimental results, Preprints, 16th Radar Meteorology Conference, Amer. Meteor. Soc., Boston, pp 337-340.

4. Frisch, A. S., and Strauch, R. G. (1976) Doppler radar measurements of eddy dissipation rates in a northeastern Colorado convective storm, J. Appl. Meteor. 15:1012-1017.

5. Lee, J. T. (1977) Application of Doppler Weather Radar to Turbulence Measurements Which Affect Aircraft, Final Report FAA-RD-77-145 to Systems Research and Development Service, FAA., Washington, D.C.

6. Pruppacher, H. R. and Klett, J. D. (1978) Microphysics of Clouds and Precipitation, D. Reidel Publishing Co., Boston.

7. Stackpole, J. D. (1961) The effectiveness of raindrops as turbulence sensors, Proceedings 9th Weather Radar Conference, Amer. Meteor. Soc., Boston, pp 212-217.

8. Rogers, R. R., and Tripp, B. R. (1964) Some radar measurements of turbulence in snow, J. Appl. Meteor. 3:603-610.

9. Srivastava, R. C., and Atlas, D. (1974) Effect of finite radar pulse volume on turbulence measurements, J. Appl. Meteor. 13:472-480.

10. Frisch, A. S., and Clifford, S. F. (1974) A study of convection capped by a stable layer using Doppler radar and acoustic echo sounders, J. Atmos. Sci. 31:1622-1628.

11. Doviak, R.J., Sirmans, D., Zrnic, D., and Walker, C.R. (1978) Considerations for pulse Doppler radar observations of severe thunderstorms, J. Appl. Meteor. 17:189-205.

12. MacCready, P. (1964) Standarization of gustiness values from aircraft, J. Appl. Meteor. 3:439-449.

13. Atlas, D., and Srivastava, R.C. (1971) A method for radar turbulence detection, IEEE Trans. on Aerospace and Electronics, AES-7, No. 1, pp 179-187.

14. Sychra, J. (1974) Fluctuation Spectra and Velocity Structure Function, Tech. Rpt. 33, Lab. Atmos. Prob., U. of Chicago.